THEORETICAL ANALYSIS OF ERRORS WHEN ESTIMATING SNOW DISTRIBUTION THROUGH POINT MEASUREMENTS

By

Ernesto Trujillo[1, 2] and Michael Lehning[2, 1]

1. School of Architecture, Civil and Environmental Engineering, École Polytechnique Fédérale de Lausanne, Lausanne, Switzerland

2. WSL Institute for Snow and Avalanche Research SLF, Davos, Switzerland

Corresponding Author:

Ernesto Trujillo
EPFL ENAC IIE CRYOS, Station 2
Lausanne, Switzerland, CH-1015
Email: Ernesto.Trujillo@epfl.ch
Office: +41 21 693 5938

Abstract

In recent years, marked improvements in our knowledge of the statistical properties of the spatial distribution of snow properties have been achieved thanks to improvements in measuring technologies (e.g., LIDAR, TLS, and GPR). Despite this, objective and quantitative frameworks for the evaluation of errors in snow measurements have been lacking. Here, we present a theoretical framework for quantitative evaluations of the uncertainty in average snow depth derived from point measurements over a profile section or an area. The error is defined as the expected value of the squared difference between the real mean of the profile/field and the sample mean from a limited number of measurements. The model is tested for one and two dimensional survey designs that range from a single measurement to an increasing number of regularly-spaced measurements. Using high-resolution (~ 1m) LIDAR snow depths at two locations in Colorado, we show that the sample errors follow the theoretical behavior. Furthermore, we show how the determination of the spatial location of the measurements can be reduced to an optimization problem for the case of the predefined number of measurements, or to the designation of an acceptable uncertainty level to determine the total number of regularly-spaced measurements required to achieve such error. On this basis, a series of figures are presented as an aid for snow survey design under the conditions described, and under the assumption of prior knowledge of the spatial covariance/correlation properties. With this methodology, better objective survey designs can be accomplished that are tailored to the specific applications for which the measurements are going to be used. The theoretical framework can be extended to other spatially distributed snow variables (e.g., SWE) whose statistical properties are comparable to those of snow depth.

1 Introduction

The assessment of uncertainties of snow measurements remains a challenging problem in snow science. Snow cover properties are highly heterogeneous over space and time and the representativeness of measurements of snow stage variables (e.g., snow depth, snow density, and snow water equivalent (SWE)) is often overlooked due to difficulties associated with the assessment of such uncertainties. This has been, at least in part, due to the limited knowledge of the characteristics of the spatial statistical properties of variables such as snow depth and SWE, particularly at the small-scales (sub-meter to tens of meters). However, recent improvements in remote sensing of snow (e.g., light detection and ranging (LiDAR) and Radar technologies) have allowed significant progress in the quantitative understanding of the small-scale heterogeneity of snow covers in different environments (e.g., Trujillo et al., 2007; Trujillo et al., 2009; Mott et al., 2011).

Point or local measurements of snow properties will continue to be necessary for purposes ranging from inexpensive evaluation of the amount of snow over a particular area, to validation of models and remote sensing measurements. Such measurements have a footprint representative of a very small area surrounding the measurement location (i.e., support, following the nomenclature proposed by Blöschl (1999)), and the integration of several measurements is necessary for a better representation of the snow variable in question over a given area. Because of this, tools for quantitative evaluations of the representativeness and uncertainty of measurements need to be introduced, and the uncertainty of such measurements should be more widely discussed in the field of snow sciences.

Currently, efforts to assess the reliability and uncertainty of snow measurements have focused on statistical analyses using point measurements (e.g., Pomeroy and Gray, 1995; Yang

66 and Woo, 1999; Watson et al., 2006; Rice and Bales, 2010; Lopez-Moreno et al., 2011; Meromy
67 et al., 2013) or synthetically generated fields in a Monte Carlo framework (e.g., Kronholm and
68 Birkeland, 2007; Shea and Jamieson, 2010), comparisons between remotely sensed and ground
69 data (e.g., Chang et al., 2005; Grünewald and Lehning, 2014), and analyses of subsets drawn
70 from spatially distributed remotely sensed data (e.g., McCreight et al., 2014). These studies have
71 been useful to empirically quantify uncertainties associated with point measurements. For
72 example, Pomeroy and Gray (1995) present an equation for determining the minimum number of
73 surveys points required to be confident that the mean falls within a certain envelop around the
74 sample mean based on the CV of SWE or snow depth. McCreight el al. (2014) use the NASA's
75 Cold Land Processes Experiment (CLPX) LIDAR snow depth dataset (also used in this study) to
76 empirically address questions regarding the inference of larger-scale snow depths from sparse
77 observations. They evaluate estimation uncertainty from random sampling for varying sample
78 size. Their conclusions indicate that adding observations to a randomly distributed survey pattern
79 leads to a reduction in both percent-error in snow volume over the study areas, as well as its
80 uncertainty. They also add that with a few hundred observations, one can expect to infer the true
81 mean snow depth over the 1-km^2 domains to within 2% error. Despite of these insights, these
82 type of empirical approaches can be site-dependent, they do not provide a theoretical quantitative
83 framework for the assessment of uncertainties associated with a particular sampling design, they
84 do not allow for an optimal sampling strategy (e.g., selecting the number of points and locations
85 for a desired accuracy level), and they do not take advantage of the increased knowledge of the
86 characteristics of the heterogeneity of snow cover properties.

87 Another possible approach is one in which the expected error in the estimation of a particular
88 statistical moment of a field over a defined domain (e.g., areal mean or standard deviation from a

89 finite number of measurements) is determined on the basis of known statistical properties of the
90 field in question. Such approach uses geostatistical principles that have been proposed by
91 Matheron (1955; 1970) and others, and that have been applied in mining geostatistics (Journel
92 and Huijbregts, 1978), the analysis of uncertainties in measuring precipitation (Rodríguez-Iturbe
93 and Mejía, 1974), and for a more general analysis of the effects of sampling of random fields as
94 examples of environmental variables (e.g., Skøien and Blöschl, 2006). Implementation of these
95 types of approaches appear to be lacking in the numerous studies using point measurements to
96 represent snow distribution. Often in these studies, the spatial snow distribution derived from
97 point measurements is addressed as the "true" distribution, which is then used for evaluating the
98 performance of interpolation methodologies, regressions trees, and hydrological models. These
99 comparisons ignore the intrinsic error incurred when extrapolating the original point
100 measurements, leaving a proportion of uncertainty unaccounted for that can be significant. The
101 the principal motivation of the present study is to encourage the use of more objective and
102 quantitative methodologies for error evaluation in snow sciences. The approach presented below
103 can be used for objective survey design to estimate snow distribution from point measurements.
104 We do not intend to present our approach as novel in the general geostatistical sense; instead, we
105 present the derivation with the specific application for snow sciences in mind. However, because
106 of the general nature of the random fields' theory the development is based on, similar
107 developments can indeed be applied to other environmental variables that can be described as a
108 random field.

109 On this basis, the error in the estimation of spatial means from point measurements over a
110 particular domain (e.g., a profile, or an area) can be quantified as the expected value of the
111 squared difference between the real mean and the sample mean obtained from a limited number

112 of point measurements. Such an approach, as it will be shown here, uses spatial statistical
113 properties of snow depth fields in a way that allows for an objective evaluation of the estimation
114 error for snow depth measurements. The sections below illustrate the use of such methodology
115 for optimal design of sample strategies in the specific context of snow depth. However, the
116 methodology can also be implemented for other snow variables such as snow water equivalent.

117 ## 2 Background

118 Let $Z(\mathbf{x})$ denote a random field function of the coordinates **x** in the *n*-dimensional space
119 $\mathbb{R}^n$. Bold letters represent a location vector from hereon. In our case, the field can represent e.g.:
120 snow depth or snow water equivalent (SWE) at a given time of the year. The mean of the process
121 over a domain *A* (e.g., a profile section or an area) is defined as:

122 $$\mu_z(A) = \frac{1}{A}\int_A z(\mathbf{x})d\mathbf{x} \qquad (1)$$

123 In practice, the mean is often obtained from the arithmetic average of measurements at a
124 finite number of locations, *N*, within the domain:

125 $$\overline{Z} = \frac{1}{N}\sum_{i=1}^{N} z(\mathbf{x}_i) \qquad (2)$$

126 The performance of the estimator $\overline{Z}$ can be evaluated by calculating the expected value of
127 the square difference between the estimator $\overline{Z}$ and the true mean $\mu_z(A)$

128 $$\sigma^2_{\overline{Z}}(A) = E\left[\left(\frac{1}{N}\sum_{i=1}^{N} z(\mathbf{x}_i) - \frac{1}{A}\int_A z(\mathbf{x})d\mathbf{x}\right)^2\right] \quad (3)$$

For a 1st order stationary process (i.e., the mean independent of location; e.g., Cressie (1993), section 2; and Journel and Huijbregts (1978), section 2), (3) can be expressed as

$$\sigma_{\bar{Z}}^2(A) = \frac{1}{N^2}\sum_{i=1}^{N} VAR\left[z(\mathbf{x}_i)\right] + \frac{2}{N^2}\sum_{i=1}^{N-1}\sum_{j=i+1}^{N} COV\left[z(\mathbf{x}_i)z(\mathbf{x}_j)\right]$$
$$-\frac{2}{N\cdot A}\sum_{i=1}^{N}\int_A COV\left[z(\mathbf{x}_i)z(\mathbf{x}_j)\right]d\mathbf{x}_j \qquad (4)$$
$$+\frac{1}{A^2}\int_A\int_A COV\left[z(\mathbf{x}_i)z(\mathbf{x}_j)\right]d\mathbf{x}_i\, d\mathbf{x}_j$$

where VAR[ ] and COV[ ] are the variance and the covariance, respectively. If we further assume that the process is second order stationary (e.g., Cressie (1993), section 2; and Journel and Huijbregts (1978), section 2), that is, if the mean and the variance are independent of the location, and the covariance function depends only on the vector difference $\mathbf{x}_i - \mathbf{x}_j$, . (3) can be expressed as

$$\sigma_{\bar{Z}}^2(A) = \sigma_p^2\left[\begin{array}{l} \frac{1}{N} + \frac{2}{N^2}\sum_{i=1}^{N-1}\sum_{j=i+1}^{N} CORR\left[\mathbf{x}_i - \mathbf{x}_j\right] \\ -\frac{2}{NA}\sum_{i=1}^{N}\int_A CORR\left[\mathbf{x}_i - \mathbf{x}_j\right]d\mathbf{x}_j \\ +\frac{1}{A^2}\int_A\int_A CORR\left[\mathbf{x}_i - \mathbf{x}_j\right]d\mathbf{x}_i\, d\mathbf{x}_j \end{array}\right] \qquad (5)$$

where CORR[ ] is the correlation function, and σ_p^2 is the variance of the point process.

The first two terms in (5) are the total sum of the covariances (or correlation as σ_p^2 has been factored out) between all point locations $i = 1,\ldots,N$ (e.g., measurement locations). The first of the two terms is only a function of the number of points, while the second is a function of the number of points, *N*, and the correlations between the locations. Such correlations are themselves

143 a function of the separation vectors (both in magnitude and direction), and the parameters of the
144 correlation function. These two terms are independent of the size of the area A, and can be
145 thought of as the portion of the error caused by the correlation between the point processes at the
146 locations $i = 1,\ldots,N$ (e.g., measurement locations). Term 3 accounts for the correlation between
147 the measurement locations and the continuous process over the domain A. This term can be seen
148 as a negative contribution to the total error assuming that the sum of the integrals is positive. The
149 term is a function of the number of points, N, the domain area, A, the location of the points and
150 the correlation structure, characterized using the parameters of the correlation function. Lastly,
151 term 4 is the contribution to the error caused by the intrinsic correlation structure of the
152 continuous process over the domain. This term is a function of the domain (e.g., size and shape
153 of A) and the correlation structure (e.g., parameters of the correlation function).

154 # 3 Data

155 For the analyses and tests of the methodology presented here, Light Detection and Ranging
156 (LIDAR) snow depths obtained as part of the NASA's Cold Land Processes Experiment (CLPX)
157 will be used (Cline et al., 2009). The dataset consists of spatially distributed snow depths for 1-
158 km x 1-km areas (Intensive Study Areas - ISAs) in the Colorado Rocky Mountains close to
159 maximum snow accumulation in April, 2003. The data were processed from snow-on (8-9 April,
160 2013) and snow-off (18-19 September, 2013) LIDAR elevation returns with an average
161 horizontal spacing of 1.5 m and vertical tolerance of 0.05 m. The final CLPX snow depth
162 contour product (0.10 m vertical spacing) was generated from these returns. This product was
163 used to generate gridded snow depth surfaces with 1024x1024 elements over the ISAs, for a grid
164 resolution of 0.977 m. For this study two areas will be used: the Fraser – St Louis Creek ISA
165 (FS) and the Rabbit Ears – Walton Creek ISA (RW) (Figure 1). The FS ISA is covered by a

166 moderate density coniferous (lodgepole pine) forest on a flat aspect with low relief. The RW ISA
167 is characterized by a broad meadow interspersed with small, dense stands of coniferous forest
168 and with low rolling topography. The snow depth distributions in these ISAs show differences
169 that are relevant for the analysis of the methodology introduced here. At the FS ISA, the snow
170 depth distribution is relatively isotropic (Figure 1b), with short spatial correlation memory and
171 little variations in the spatial scaling properties (i.e., power-spectral exponents and scaling
172 breaks) with direction (Trujillo et al., 2007). On the other hand, the spatial distribution of snow
173 depth in the RW ISA is more anisotropic (Figure 1c), with longer spatial correlation memory
174 along a principal direction aligned with the predominant wind direction versus shorter memory
175 along the perpendicular direction, and with variations in the power-spectral exponents and
176 scaling breaks according to the predominant wind directions (Trujillo et al., 2007).

177 # 4 One-dimensional process

178 The spatial representation of the snow cover requires a basic assumption on the scale or
179 resolution at which a field or profile is going to be represented. This relies on the spatial support
180 of the measurements. For the case of snow depths, point measurements from local surveys using
181 a snow depth probe are frequently used for this representation. Generally, there are additional
182 sources of uncertainty associated with these types of measurements, such as the accuracy of the
183 position of the measurement in space or deviations in the vertical angle of penetration of the
184 probe through the snow pack. These uncertainties are additional to any of the uncertainties
185 estimated using the methodology discussed here.

186 The one-dimensional case provides a good opportunity to illustrate the limitations of point
187 measurements. Consider the case of a snow depth profile that is measured using a snow depth
188 probe at a regular spacing “d”. Each of these point measurements is meant to represent the mean

189 snow depth over a particular distance surrounding the measurement. The question is: over what
190 distance is this assumption valid? In this case, the intrinsic assumption is that the measurement is
191 representative over the distance "d", but at this point the validity of such an assumption is not
192 proven.

193 The answer to this question is conditioned to how variable the profile is and over what
194 distances. To address this, let us look at two snow depth profiles, one in a forested environment
195 (FS) and another in an open environment (RW) in the Colorado Rocky Mountains (Figure 2a and
196 Figure 3a, respectively). The variability in the profiles is markedly different, with variations over
197 shorter distances in the forested area, and a smoother profile in the open and wind influenced
198 environment. This is reflected in the spatial correlation structure of these snow depth profiles,
199 with stronger correlations over longer distances in open and wind-influenced environments with
200 respect to that in forested environments (Trujillo et al., 2007; Trujillo et al., 2009). These
201 differences should be considered when selecting the sampling frequency required to capture the
202 variability and accurately represent the mean conditions within a particular sampling spacing.
203 This is illustrated by comparing the mean snow depth for a particular resolution to the point
204 value at the center of the interval (Figure 2b in a forested environment and Figure 3b in an open
205 and wind-influenced environment). In the Figures, average versus point values at several
206 sampling intervals are compared for normalized profiles ($\mu = 0$, $\sigma = 1$) separated every 30 m in
207 both the x (east) and y (north) directions and for an area of 500 m by 500 m. The 30-m separation
208 between profiles is chosen to reduce the spatial correlation between them.

209 Firstly, the resulting comparison shows that the point values generally overestimate the
210 variability in mean snow depths if we replace the mean snow depth distribution by its point
211 sample. To clarify this, let us consider here two snow depth profiles, one with the snow depths at

212 the nominal scale (~1 m), and a second one with a moving average (MA) of the first one with an
213 averaging window equal to the sampling spacing. Ultimately, the variance/standard deviation of
214 the first profile (~1 m) is larger than that of the MA, with a distribution that reflects these
215 differences. The samples drawn from the first profile will reflect a larger variance than that of the
216 samples from the MA profile as they are drawn from these distributions, and this is what is
217 reflected in Figure 2 and Figure 3. The degree of overestimation can be quantified through the
218 slope of the regression line (in red in Figure 2b and Figure 3b). In the forested environment
219 (Figure 2b), the slopes range between 0.8 and 0.13, with decreasing slopes with increasing
220 spacing. These slopes indicate that, on average, the mean values are 0.8 times the point values
221 for the 5 m spacing and 0.1 times the point values for the 100 m spacing. In the open and wind-
222 dominated environment, the slopes are higher and range between 0.97 and 0.23 from 5 m spacing
223 and 100 m spacing, respectively. A clear difference emerges: forested environments require
224 shorter separation between single measurements if the snow depth profile is to be accurately
225 captured by the measurements. The variability within the size of the interval determines the
226 degree of uncertainty associated with the point measurements, as the sub-interval variability is
227 related to the degree of overestimation of the mean value within the interval.

228 Secondly, the differences between average and point values for each spacing distance are
229 generally more scattered in the forested environment than in the open environment, and in both
230 environments the degree of scattering increases with spacing (Figure 2c and Figure 3c).
231 However, it is important to note here that we are comparing normalized profiles ($\mu = 0$, $\sigma = 1$),
232 allowing us to focus on the rescaled spatial variations. What is highlighted is the relevance of the
233 spatial structure of the profile rather than the absolute variance. This spatial structure can be
234 quantified by, for example, the spatial covariance/correlation function.

In addition to differences in correlation structure, there are also differences in the absolute variability in snow depth in these environments (Figure 4). Contrary to the normalized snow depth discussed above, the subinterval standard deviation as a function of interval size along the profiles is higher in the open and wind-influenced environment at RW versus the forested environment at FS (Figure 4a). Mean standard deviation values in the open environment are twice as large as those at the forested environment towards the larger interval sizes (~100 m). The standard deviation increases with interval size in both environments, with the steepest increase at the lower interval sizes. Furthermore, the standard deviation tends to stabilize more rapidly in the forested environments, with an increase of only 1.8 cm between 30 m and 100 m. On the other hand, the standard deviation continues to increase in the open environment at RW, with less of an asymptotical behavior for the scales analyzed. Complementary, the shaded areas (25% to 75% quantiles) give an idea of the variability of standard deviation values, with a much wider range in RW versus FS, and an increase in the range between quantiles with interval size in RW.

Consistent with the standard deviation, the sub-interval mean range (range defined as the difference between the maximum and minimum snow depths within an interval) increases with interval size in both FS and RW (Figure 4b). However, the mean range is larger in the open environment at RW and the rate of increase with interval size is also steeper. Similarly, the shaded areas indicate wider distribution of range values in the open environment at RW, while relatively uniformly distributed around the mean across interval sizes in the forested environment at FS. The results in Figure 2-Figure 4 illustrate this contrasting behavior between the snow covers in these environments and their influence on measurement strategies: that is, the forested environments requires shorter separation between measurements for accurate representation of

the snow cover, however, in the wind-influence and open environment, the subinterval variability is higher indicating wider variations around any sampled measurement within the interval.

Ultimately, the number and distance between measurements and the specific arrangement of the measurements are all conditioned to what the measurements are needed for. Hydrologic applications may not require a highly detail representation of a snow depth profile (or a field), and representing the average conditions over a given distance (or area) is sufficient, but small-scale process-based studies may require a more detailed characterization over shorter distances (or smaller areas). This implies that the decision depends on the particular use that the measurements will support. In the following sections, the equations presented in the Background (section 2) will be applied to evaluate the uncertainty associated with multiple measurement designs for profiles and fields of snow depth.

4.1 Case 1: Single measurement along a profile section

Equation (2) can be used to evaluate the uncertainty of a single measurement along a profile section of length L. For this case, as well as for the following cases in this article, an exponential covariance with a decay exponent v ($v > 0$) will be assumed:

$$COV(\mathbf{h},\sigma,v) = \sigma^2 \exp\left(-v\left|\left|\mathbf{h}\right|\right|\right) \quad \text{for } \sigma^2 > 0, \text{ and } v > 0 \qquad (6)$$

were σ^2 is the variance, and $\left|\left|\mathbf{h}\right|\right|$ is the length of the vector $\mathbf{h}$. For this one-dimensional case and combining (6) and (5), the following expression is obtained:

$$\sigma^2_{\bar{Z}}(x,L,v)\Big/\sigma^2_p = 1 - \frac{2}{Lv}\left[2 - \exp(-vx) - \exp\left(-v\cdot\left[L-x\right]\right)\right] + \frac{1}{L^2 v}\left[2L + \frac{2}{v}\exp(-vL) - \frac{2}{v}\right] \qquad (7)$$

where x is the distance from one extreme of the section to the location of the measurement (Figure 5a). The normalized squared error $\sigma^2_{\bar{Z}}(x,L,v)/\sigma^2_p$ is minimized at x equal to half of the section length, $L/2$, regardless of v. The existence of a correlation in the profile leads to this solution, as the middle location contains more information about its surroundings. Also, this solution is different from the solution for an uncorrelated profile (e.g., white noise), for which the squared error would be equal to the variance, independent of the location of the measurement.

The results here are confirmed with an analysis of LIDAR snow depths profiles in FS and RW (Figure 6). The analysis consists of calculating the difference between the mean and the point value for sections of a given length (varied between 10 m – 50 m) and for x (Figure 5a) between 0 and L along the profile sections. Each sample section of length L will provide a single difference for each of the x values. These sample differences are then used to calculate the mean normalized squared error for each x, and the same is repeated for each section length L. The results indicate that the real snow depth profiles behave as predicted by the model of the error, with a minimum error at x equal to half of the section length. Another difference highlighted by these results is the difference between the sample errors in the forested environment (FS) versus the open environment (RW) for the larger interval sizes (e.g., 50 m). The sampled normalized squared error in the forested environment shows only a mild decrease in the square error to around 0.7-0.8 towards the inside of the section length. However, this decrease is achieved for the measurement along most of the interval length with the exception of the extremes. This can be explained by the relationship between the spatial memory of snow depth (e.g., the correlation function) and the section length. Densely forested environments exhibit correlation lengths that are shorter than those in open and wind influenced environments (e.g., Trujillo et al., 2007;

302 Trujillo et al., 2009). As the section length increases beyond such correlation lengths, a
303 measurement location towards the middle of the interval contains less information of the
304 surrounding snow depths in a forested environment (e.g., FS) versus an open and wind
305 influenced environment (e.g., RW). This is observed in Figure 6c versus Figure 6f, with the
306 results in RW showing a more clear minimum towards the center of the profile section. The
307 results also show a poorer performance of the model in RW versus FS, as the exponential
308 correlation model has a poorer fit in RW at the shorter-lag range; However, model performance
309 is improved for longer section lengths (e.g., Figure 6c and f)

310 Model and sampled results thus support that the measurement location can be fixed in the
311 middle of the interval, and the normalized squared error can then be described as a function of
312 both the exponential decay exponent, v, and the length of the section, L (Figure 7a). The
313 normalized squared error increases with interval length, with a steeper increase for larger
314 exponential decay exponents, for which the squared error approaches that of an uncorrelated
315 field more rapidly. The theoretical model is tested on the snow depth fields at FS and RW. The
316 test consists of calculating the sampled normalized squared error as the average of all squared-
317 differences between the mid-section snow depth and the mean from all LIDAR grid-points
318 within each interval of length L. This is done for profiles separated every 30 m, similar to the
319 analysis above, and for profiles along the x and y directions. The theoretical normalized squared
320 error is estimated from (7) using the exponential decay exponent from the model fitted to the
321 sampled correlation function. The results show that the theoretical model reproduces the sampled
322 squared error remarkably well, even reproducing the anisotropic properties of the correlograms,
323 represented by the different exponents of the exponential model along x and y directions (Figure
324 7b and c). The model also reproduces the different behavior of the squared error between both

fields (i.e., FS and RW), showing that the normalized squared error increases more rapidly and is larger in the forested environment (Figure 7b) versus the open environment (Figure 7c). However, it should be noted here that as the error is normalized and as the variance of the field in the open environment is larger (Figure 4a), the absolute squared error could reach higher values in the open environment (RW). In this regard, one feature to discuss here is the assumption that the point variance of snow depth in these environments has been estimated as the spatial variance over the entire study area, as it is generally practiced in time series analysis and geostatistics. In practice, this is the only possible approach because there is limited information to estimate the point variance from multiple realizations of the process at each spatial location, as inter- and intra- annual snow depth fields are not available, not only for these areas, but for almost any area where this methodology may be applied.

4.2 Case 2: Three measurements along a profile section

From (5) it is also evident that increasing the number of measurements will reduce the squared error. In the case of three measurements separated by a distance 'a', with the middle measurement centered in the section of length L (Figure 5b), and for an exponential covariance function with parameter v, (5) leads to the following expression for this particular case:

$$\begin{aligned}\sigma^2_{\bar{Z}}(a,L,v)\big/\sigma^2_p = {} & \frac{1}{3}+\frac{2}{9}\left[2\exp(-va)-\exp(-2va)\right] \\ & -\frac{4}{3Lv}\left[3-\exp\left(-\frac{vL}{2}\right)\left(1+\exp(-va)+\exp(va)\right)\right] \\ & +\frac{1}{L^2v}\left[2L+\frac{2}{v}\exp(-vL)-\frac{2}{v}\right]\end{aligned} \tag{8}$$

Equation (8) can be minimized to determine the optimal separation distance between points, a, as a function of L and v:

$$a_{optimal} = -\frac{1}{\nu}\ln(t) \qquad (9)$$

where

$$t = \frac{B + \sqrt{B^2 - 4AB}}{2A}$$

$$A = \frac{4\nu}{9}$$

$$\text{and } B = -\frac{4}{3L}\exp\left(-\frac{\nu L}{2}\right)$$

The combination of (8) and (9) can be used to determine the normalized squared error, $\sigma_{\bar{Z}}^2 / \sigma_p^2$, and the optimal distance, $a_{optimal}$, for the measurement pattern in Figure 5b. The model predicts that the normalized squared error is minimized at an intermediate location between 0 and $L/2$ (black lines in Figure 8a and b). The results show an increase in the error with interval size, L, as well as little sensitivity of $a_{optimal}$ to ν. This latter feature can be seen as an advantage since small biases in the estimation of ν will not result in significant biases in the estimation of $a_{optimal}$. One could almost assume a value of $a_{optimal}$ without prior knowledge of the exponential decay exponent, selecting $a_{optimal}$ within the range of values indicated by the model for a rage of possible exponential decay exponents. Note that $a_{optimal}$ is located close to the 60% distance from the center towards the outer boundary of the profile section for all section lengths (Figure 8a and b). On the other hand, the measurement error displays a higher sensitivity to ν around $a_{optimal}$, indicating that biases in the estimation of ν would have a more noticeable effect on the estimation of the measurement error. This is further clarified in Figure 8c, in which the normalized error (not squared) and $a_{optimal}$ can be obtained for corresponding profile section

363 lengths (L) and exponential decay exponents (v) based on the isolines shown. For example, for a
364 profile section of 30 m, and an exponential decay exponent of 0.2 m^{-1}, the normalized error is
365 0.32 and $a_{optimal}$ is 9.63 m (see intersect of the two isolines in Figure 8c). The normalized error in
366 Figure 8c is not squared, highlighting the sensitivity of the measurement error to v, which
367 represents the degree of spatial correlation of the profile in this case (e.g., lower values indicate
368 stronger spatial memory/correlation, hence lower measurement errors).

369 The performance of the model is tested against the normalized squared error obtained from
370 the same snow depth profiles in FS and RW. The test consists of estimating the normalized
371 squared error for profiles sections of length between 10 m and 80 m, with a being varied between
372 0 and $L/2$ (Figure 9). For each value of a, the normalized squared error is estimated based on the
373 means obtained using the three snow depth samples for each section. All squared differences are
374 then averaged to obtain the values presented in the Figure. Sampled and modeled errors follow
375 the same trend across all a values and for the different L values in Figure 9. The minimum error
376 is also reproduced by the model proving the applicability of the model for estimating the optimal
377 separation between measurements. The model does perform better in the forested environment of
378 FS versus RW, particularly for lower a values. This can be justified as the exponential
379 covariance model displays a better fit in FS over RW, particularly over the lower range of lag
380 values. Also, note that both the modeled and sampled normalized squared errors are lower for the
381 snow depth profiles at RW because of the longer spatial memory of the snow depth distribution
382 in this environment (higher spatial correlations) when compared to that in FS.

383 **4.3 Case 3: *N* measurements along a profile section**

384 As stated above, the measurement error can be reduced by increasing the number of
385 measurements taken over a given section of length L. Let us focus on the case of stratified

sampling where N regularly spaced measurements are taken over the interval (Figure 5c), and to quantify this reduction we can use (5) and the exponential covariance model. Equation (5) can then be reduced to:

$$\sigma_{\bar{Z}}^2(N,L,v)/\sigma_p^2 = \frac{1}{N} + \frac{2}{N^2}\sum_{k=1}^{N-1} k\exp\left(-v\left[L - kL/N\right]\right) - \frac{4}{Lv}\left[1 - \frac{1}{N}\sum_{k=1}^{N}\exp\left(-v\frac{L}{N}\left[N - k + 1/2\right]\right)\right] - \frac{2}{L^2v^2}\left[1 - Lv - \exp(-vL)\right] \quad (10)$$

The normalized squared error ($\sigma_{\bar{Z}}^2/\sigma_p^2$) obtained with (10) for profiles sections of lengths between 10 and 80 shows a steep decrease with N (Figure 10), with a steeper decrease for higher exponential decay exponents. For the longer profile sections (e.g., 80, Figure 10d), small reductions in the squared error are achieved beyond only a few measurements (e.g., N = 16). Equation (10) and the results in Figure 10 can be used to determine the number of measurements necessary to achieve a desired accuracy level. One could, for example, design a survey to sample a snow depth profile with a mean value every 10 m. The number of measurements required to achieve a desired level of accuracy can be obtained from Figure 10a, based on previous knowledge of the sample estimate of the exponential decay exponent. This can be achieved thanks to the intra-annual and inter-annual persistence of the spatial patterns, and hence, the spatial statistical properties of snow depth fields in mountain environments, as shown in previous studies using both manual surveys and LIDAR measurements (e.g., Deems et al., 2008; Sturm and Wagner, 2010; Schirmer et al., 2011; Melvold and Skaugen, 2013; Helfrich et al., 2014). A detailed spatial survey (e.g., dense manual measurements or TLS), sampling different portions of an area can be used to determine the covariance/correlation characteristics of the snow depth

405 distribution, with which the model for the error can be applied. An a priori estimate of the
406 exponential decay exponent may also be possible and will be tested in future applications of the
407 framework, given the relative insensitivity of the error with respect to v.

408 Following the method described in the previous section, we test the performance of the
409 model against the normalized squared error obtained from the same snow depth profiles in FS
410 and RW. In this case, the sampled squared error is estimated based on the N regularly-spaced
411 measurements distributed along the profile sections of length L. As the snow depth fields are
412 gridded at ~1-m resolution, the location of the measurements is approximated to the closest
413 coordinate in the profile section following the pattern in Figure 5c. Once again, sampled and
414 modeled errors follow closely the same trend for the different L values in both FS and RW
415 (Figure 11). The error decreases with N, with a rapid decay at the lower N values, illustrating that
416 the error can be drastically reduced by simply increasing the number of measurements by a small
417 amount. The normalized squared error across all N values is lower for RW than for FS,
418 consistent with the higher spatial correlations observed in the snow depth fields of RW versus
419 FS. Once again, there are some differences between the sampled and modeled normalized
420 squared error in RW for the shorter profile lengths and for small N values: a consequence of the
421 poorer fit of the exponential model for the shorter lag range in RW. However, the model is still
422 able to reproduce the error in both fields, and the applicability of the model is illustrated even
423 when the fit of the correlation model can be improved.

424 ## 5 Two-dimensional process

425 Similar to the one-dimensional process, equation (5) can be formulated to calculate the
426 squared error in the two-dimensional space. To exemplify this, we apply the methodology to an
427 isotropic process over the x-y plane for three cases in a square area: (a) one single measurement

428 in the center of the area, (b) five measurements radiating out from the center (Figure 12a), and
429 (c) N by N measurements regularly spaced in the x and y directions (Figure 12b).

430 For the isotropic case, the covariance/correlation function is only dependent on the
431 magnitude of the lag vector,

432 $$h_{i,j} = \left| \mathbf{x}_i - \mathbf{x}_j \right| \qquad (11)$$

433

434 and, consequently, the error is represented by,

435 $$\sigma_{\bar{Z}}^2(A) = \sigma_p^2 \left[\begin{array}{l} \frac{1}{N} + \frac{2}{N^2} \sum_{i=1}^{N-1} \sum_{j=i+1}^{N} CORR\left[h_{i,j}\right] \\ -\frac{2}{NA} \sum_{i=1}^{N} \int_A CORR\left[h_{i,j}\right] d\mathbf{x}_j \\ +\frac{1}{A^2} \int_A \int_A CORR\left[h_{i,j}\right] d\mathbf{x}_i \, d\mathbf{x}_j \end{array} \right] \qquad (12)$$

436

437 The exponential correlation function for the isotropic case takes the following form:

438 $$CORR(h,\nu) = \exp(-\nu h) \quad (13)$$

439 where h is the magnitude of the lag vector. Replacing into the expression for $\sigma_{\bar{Z}}^2$, we obtain,

440 $$\sigma_{\bar{Z}}^2 = \sigma_p^2 \left[\begin{array}{l} 1/N + 2/N^2 \sum_{i=1}^{N-1} \sum_{j=i+1}^{N} \exp\left(-\nu \left| \mathbf{x}_i - \mathbf{x}_j \right|\right) \\ -2/NA \sum_{i=1}^{N} \int_A \exp\left(-\nu \left| \mathbf{x}_i - \mathbf{x}_j \right|\right) d\mathbf{x}_j \\ +1/A^2 \int_A \int_A \exp\left(-\nu \left| \mathbf{x}_i - \mathbf{x}_j \right|\right) d\mathbf{x}_j \, d\mathbf{x}_i \end{array} \right] \qquad (14)$$

For the case of a rectangular area of side dimension L_x and L_y in the corresponding x and y directions, the equation becomes,

$$\sigma_{\bar{Z}}^2 = \sigma_p^2 \left[\begin{array}{l} 1/N + 2/N^2 \sum_{i=1}^{N-1} \sum_{j=i+1}^{N} \exp\left(-v\left(\left(x_i - x_j\right)^2 + \left(y_i - y_j\right)^2 \right)^{1/2} \right) \\ -2/NA \sum_{i=1}^{N} \int_0^{L_y} \int_0^{L_x} \exp\left(-v\left(\left(x_i - x\right)^2 + \left(y_i - y\right)^2 \right)^{1/2} \right) dx\, dy \\ + 1/A^2 \int_0^{L_y} \int_0^{L_x} \int_0^{L_y} \int_0^{L_x} \exp\left(-v\left(\left(x' - x\right)^2 + \left(y' - y\right)^2 \right)^{1/2} \right) dx\, dy\, dx'\, dy' \end{array} \right] \quad (15)$$

The limits of the integrals can be changed depending on the desired location of the origin. In this case, the origin is located at the lower-left corner.

As discussed earlier, the first term is only a function of N, such that the base error is the variance of the point process divided by the number of points. The second term is a function of N, the location of the points, and the decay rate v. The third term is a function of N, A, the location of the points, and the decay rate v. The fourth term is a function of A and v, but is independent of the location of the points and N (i.e., independent of the survey design, and only a function of the correlation structure of the continuous process).

5.1 Case 1: Single measurement in the center of the area

In this case, we focus on a single measurement in the middle of a square area of side dimension L. Numerical solution of (15) shows that the normalized squared error increases rapidly with L, with a steeper increase for higher exponential decay exponents (Figure 13a), which approach a normalized squared error of 1 for L values less than 10 (e.g., $1 \leq v \leq 5$). The theoretical results in Figure 13a can be used to determine the discrepancy between a single measurement in the middle of an area and the areal mean for a second order stationary and anisotropic process with an exponential covariance/correlation function. Comparison of the

460 modeled and sampled normalized square errors for the FS snow depth field indicate very good
461 agreement between modeled and sample errors (Figure 13b). The sample error is estimated
462 following the same procedure explained for the one-dimensional cases, although in the two-
463 dimensional space. Both sampled and modeled errors show the same behavior across L values
464 between 1 m and 100 m, although the scatter in the sampled error increases for larger L values.
465 This can be explained by the smaller number of samples to estimate the mean normalized
466 squared error and the fact that the correlation structure decays rapidly and a single sample
467 becomes less correlated to the surrounding area for these larger areas. The model introduced here
468 can then be used to assess the representativeness of a single measurement over an area
469 objectively and accurately, and it can be extended for other covariance/correlation functions as
470 needed.

471 **5.2 Case 2: Five measurements radiating out from the center of the area**

472 The case of five measurements radiating out from the center (Figure 12a), with a point in the
473 middle of the area and four points separated by a distance a from the center leads to a similar
474 optimization problem as illustrated in case 2 of the one-dimensional examples (section 4.2). In
475 the two-dimensional case, (15) does not have an explicit solution for a, and numerical
476 implementation is required. The equation can be solved by simply replacing the point
477 coordinates and the correlation function parameters. Following this approach, the normalized
478 squared error can be obtained for areas of varying sizes (Figure 14). Similar to the one-
479 dimensional example (case 2, section 4.2), $\sigma_{\bar{Z}}^2 \big/ \sigma_p^2$ decreases with a, reaching a minimum at an
480 intermediate distance from the middle point outwards. The decay in $\sigma_{\bar{Z}}^2 \big/ \sigma_p^2$ is more rapid for
481 the least correlated processes (i.e., higher decay exponents) reaching a value close to the base

482 normalized square error that is a function of the number of points (i.e., $1/N = 1/5$ in this case). An
483 extended analysis of the effect of each of the terms in the equation is included in the
484 Supplementary Information. The error, as shown in Figure 14, is minimized as a consequence of
485 two balancing terms that lead to this intermediate solution. The optimal solution is a balance
486 between reducing the correlation between the individual measurements (e.g., increasing the
487 separation between the location of the measurements) but increasing the correlation between the
488 measurements and the surrounding area (e.g., locating the measurements closer to the middle of
489 the area). These two competing effects lead to an optimization problem based on the location of
490 the point measurements. For the least correlated processes, the error resembles the behavior of an
491 uncorrelated field once the measurements become effectively decorrelated (e.g., $a > 1$ in Figure
492 14b for $v = 5$). Figure 14 exemplifies how (15) can be used to determine the optimal
493 measurement location for areas of different sizes, and to determine the associated error with
494 configurations other than the optimal.

495 The performance of the model is tested against the normalized squared error obtained from
496 the snow depth field in FS. The test consists of estimating the normalized squared error for a
497 square area with side length (L) between 10 m and 79 m, with a being varied between 0 and $L/2$
498 (Figure 15). For each value of a, the normalized squared error is estimated based on the means
499 obtained using the five snow depth samples for each section. All squared differences are then
500 averaged to obtain the values presented in the figure. Once again, the sampled and modeled
501 errors follow the same trend across all a values and for the different L values. The minimum
502 error and $a_{optimal}$ are also reproduced closely by the model, and as the area size increases, the
503 sampled and modeled error approach the error for an uncorrelated field at larger separations (i.e.,

0.2). These results illustrate that the performance of the model in the two-dimensional space is remarkable, similar to what was observed in the one-dimensional case.

5.3 Case 3: *N* by *N* measurements regularly spaced in the *x* and *y* directions

Similarl to the one-dimensional case, the two-dimensional case of N by N regularly spaced measurements (Figure 12b) leads to a decreasing normalized squared error with N (Figure 16). There is a sharp decrease in the error by just increasing the number of measurements in the lower range of N. The analysis illustrates that stratified sampling, as shown here, is an excellent approach for minimizing the error. For a 10 by 10 area for example, increasing N to 4 ($N^2 = 16$) reduces the normalized squared error to less than 0.05. It is also worth noting here that for this two-dimensional case, the error is less sensitive to the value of the exponential decay exponent (v) for the higher N values as the mean is accurately captured regardless of the correlation of the field. Beyond a certain number of measurements regularly distributed in the area, the measurements gather enough information such that there are only very minor improvements with the addition of new measurements, regardless of the exponent value. Figure 16 serves as an example of how the methodology can be used for objective selection of the number of measurements necessary to achieve a desired accuracy level using prior knowledge of the spatial covariance function.

The performance of the model is tested again for a square area with side length (L) between 10 m and 79 m using the snow depth field in FS, and for an increasing number of rows/columns of measurements leading to a total number of measurements of N^2 (Figure 17). The results illustrate again the accurate performance of the theoretical model, with sampled and model errors following closely the same squared errors. Both sampled and modeled errors increase as the size

526 of the area increases, as expected. These results complete the model performance tests for the
527 two-dimensional isotropic case.

528 6 Summary and Conclusions

529 A methodology for an objective evaluation of the error in capturing mean snow depths from
530 point measurements is presented based on the expected value of the squared difference between
531 the real average snow depth and the mean of a finite number of snow depth samples within a
532 defined domain (e.g., a profile section or an area). The model can be used for assisting the design
533 of survey strategies such that the error is minimized in the case of a limited and predetermined
534 number of measurements, or such that the desired number of measurements is determined based
535 on a predefined acceptable uncertainty level. The model is applied to one- and two-dimensional
536 survey examples using LIDAR snow depths collected in the Colorado Rockies. The results
537 confirm that the model is capable of reproducing the estimation error of the mean from a finite
538 number of samples for real snow depth fields.

539 Here, we should highlight some of the implications of the assumptions made in the model. In
540 simplified terms, the second-order stationarity assumption implies that the mean and the variance
541 of the process/variable (e.g., snow depth) are independent of the spatial location, and that the
542 covariance is dependent only on the separation vector (i.e., lag). Although these assumptions
543 may be less valid over larger scales (e.g., greater than 100 m), in the context of the model
544 application to snow depth the assumption should be valid at smaller scales. We present these
545 examples to show how the error can be quantified with good accuracy at such smaller scales.
546 Application of these types of approaches at larger scales will require additional evaluation with
547 particular attention as to what the specific demands of the application are. Also, the methodology
548 presented here is not suitable for discontinuous snow cover if both snow-covered and snow-free

549 areas are considered in the error estimation. This case has not been considered in the
550 development here.

551 Implementation of the model in practice requires prior assumption of a
552 correlation/covariance model and estimates of the model parameters (e.g., the decay exponent for
553 the exponential case). In the examples presented here we use LIDAR data for the parameter
554 estimation to illustrate the applicability of the model and its ability to estimate the error using
555 real snow depth data. Snow distributions in mountain environments have been shown to be
556 consistent intra- and inter-annually because the controlling processes are relatively consistent
557 during the season and from season to season. Such consistency suggests that the
558 correlation/covariance model should also be consistent, as well as the parameters of the model.
559 These parameters can be estimated via a dense survey either manually or with TLS of one or
560 more small plots of a size similar to the size that is aimed to be represented. These surveys would
561 not necessarily have to be repeated as the parameters and covariance models should be
562 preserved. Detailed surveys can be conducted under different conditions to characterize the range
563 of the correlation models and parameters (e.g., after a snow storm, or close to peak
564 accumulation). Also here, we should point out that although we show results for a wide range of
565 the exponential decay exponent values, we are finding that most of the values that we have
566 observed are in the lower range of those presented (e.g., 0.1-0.2 m^{-1}). Hence, the biases in the
567 estimated error and the survey design remain small.

568 Currently, remote sensing technologies (e.g., TLS, Airborne LiDAR, and ground penetrating
569 radar) are allowing for the characterization of snow cover properties at increasing resolutions in
570 both space and time. Such improvements can be utilized in the context presented here providing
571 information about the range of best fitting covariance/correlation models and parameters for

different conditions, supporting the application of methodologies such as the one presented here. With such improvements, survey designs can be optimized such that estimation errors can be explicitly addressed and accounted for, particularly when extrapolating a limited number of measurements to estimate the spatial distribution of snow. Such applications will continue to be relevant despite of the aforementioned improvements, as access to these technologies is limited by their cost and the expertise that is required for their application.

7 Acknowledgements

Data for this article was obtained from NASA's Cold Land Processes experiment (CLPX), available at http://nsidc.org/data/docs/daac/nsidc0157_clpx_lidar.

584

585 # Figures

586 Figure 1. (a) Location of the Fraser and Rabbit Ears study areas in the state of Colorado (in
587 grey). (b) LIDAR Snow depth distributions on April 8, 2003, at the Saint Louis Creek Intensive
588 Study Area (ISA) and (c) on April 9 at the Rabbit Ears ISA.

589 Figure 2. (a) Sample normalized snow depth profile (mean = 0, standard deviation = 1) in a
590 forested environment from LIDAR (1-m resolution) at the Fraser – St. Louis Creek (FS)
591 intensive study area (ISA) of the Cold Land Processes eXperiment (CLPX) (Trujillo et al., 2007;
592 Cline et al., 2009). The profile is sampled with regular separations (spacing) of 5 m, 10 m, 25 m,
593 50 m, and 100 m (from top to bottom, respectively). (b) Average values within sampling
594 intervals (same as in (a)) versus point samples for normalized snow depth profiles in the FS ISA.
595 The red line is a linear regression fit, with slope β and r^2 as indicated in each plot. (c) Histograms
596 of the difference between the point and average values for each of the sampling intervals. The
597 vertical red line marks the mean difference.

598 Figure 3. (a) As Figure 2 but for an open and wind influenced environment at the Rabbit Ears
599 – Walton Creek (RW) ISA of the CLPX (Trujillo et al., 2007; Cline et al., 2009). (b) Average
600 values within sampling intervals (same as in (a)) versus point samples for normalized snow depth
601 profiles in the RW ISA. The red line is a linear regression fit, with slope β and r^2 as indicated in
602 each plot. (c) Histograms of the difference between the point and average values for each of the
603 sampling intervals. The vertical red line marks the mean difference.

604 Figure 4. Sub-interval standard deviation (a) and range (b) for varying interval lengths for
605 profiles of snow depth in a forested environment (FS) and an open and wind-influenced
606 environment (RW) in the Colorado Rocky Mountains (same regions as those in Figure 2 and
607 Figure 3). The mean standard deviation and mean range for the study areas are shown by the
608 solid lines, while the shaded areas cover the quantiles between 25% and 75% of the values for all
609 the intervals in these areas.

610 Figure 5. Survey designs for the sampling of a snow profile.

611 Figure 6. Comparison of the theoretical and sampled normalized squared error ($\sigma_{\bar{Z}}^2/\sigma_p^2$) for
612 the case of a single measurement along a profile section of length L, as in Figure 5a. The survey
613 case applied to profiles in FS and RW along the x and y directions. Solid lines are the theoretical
614 error using exponential decay exponents derived from the functions fitted to the sampled
615 correlation functions of the two surfaces in the x and y directions.

616 Figure 7. (a) Theoretical normalized squared error for a single measurement in the middle of a
617 section of length, L, and for an exponential correlation function with a decay exponent, v. (b) and
618 (c) Comparison of the theoretical and sampled normalized squared error for the same survey case
619 applied to profiles in FS and RW along the x and y directions. Dashed lines are the theoretical
620 error from (7) using exponential decay exponents derived from the functions fitted to the
621 sampled correlation functions of the two surfaces in the x and y directions.

622 Figure 8. (a) and (b) Theoretical normalized squared error for the three-point pattern along a
623 profile section in Figure 5b, and for profile section lengths (L) of 1 (a) and 25 (b). Each of the

624 colored lines corresponds to a specific decay exponent, ν, and the black line marks the
625 theoretical solution for $a_{optimal}$. (c) Theoretical normalized error and $a_{optimal}$ for isolines of profile
626 section lengths (L) and exponential decay exponents (ν) for the three-point pattern along a profile
627 section of length L in Figure 5b.

628 Figure 9. Theoretical and sampled normalized squared error ($\sigma^2_{\bar{Z}}/\sigma^2_p$) for the three-point
629 pattern along a profile section in Figure 5b, and for profile section lengths (L) between 10 m and
630 80 m in FS and RW. The solid lines are the theoretical error from (8) using exponential decay
631 exponents derived from the functions fitted to the sampled correlation functions of the two
632 surfaces in the x and y directions, while the dots correspond to the sampled error for profiles in
633 FS (a-d) and RW (e-h).

634 Figure 10. Theoretical normalized squared error ($\sigma^2_{\bar{Z}}/\sigma^2_p$) for the N-point pattern along a
635 profile section in Figure 5c, and for profile section lengths (L) between 10 and 80 obtained from
636 (10).

637 Figure 11. Theoretical and sampled normalized squared error ($\sigma^2_{\bar{Z}}/\sigma^2_p$) for the N-point pattern
638 along a profile section in Figure 5c, and for profile section lengths (L) between 10 m and 80 m in
639 FS and RW. The solid point markers are the theoretical error from (10) using exponential decay
640 exponents derived from the functions fitted to the sampled correlograms of the two surfaces in
641 the x and y directions, while the circle markers with the dotted lines correspond to the sampled
642 error for profiles in FS (a-d) and RW (e-h).

643 Figure 12. Sample survey designs with (a) a 5-point pattern centered in the area, and (b) a
644 regularly spaced pattern. For the 5-point pattern, a can vary between 0 and $L/2$, while for the N x
645 N points pattern, the separation between the measurements is determined by the number of
646 points.

647 Figure 13. (a) Theoretical normalized squared error ($\sigma^2_{\bar{Z}}/\sigma^2_p$) for the two-dimensional case
648 with a single measurement in the middle of a square area with side dimension L. (b) Theoretical
649 and sampled normalized squared error for the same two-dimensional survey applied to the snow
650 depth field in FS. The dashed line is the theoretical error derived for an exponential decay
651 exponent of 0.17 derived from the sampled correlation function of snow depth in FS, while the
652 solid line is the sampled normalized squared error for the snow cover in FS.

653 Figure 14. Theoretical normalized squared error ($\sigma^2_{\bar{Z}}/\sigma^2_p$) as a function of the distance a from
654 the center of the area for square areas of side dimensions (L) between 10 and 80. Each curve
655 corresponds to an exponential decay (ν) between 0.1 and 5.

656 Figure 15. Theoretical and sampled normalized squared error ($\sigma^2_{\bar{Z}}/\sigma^2_p$) for the 5-point pattern
657 in Figure 12a over square areas of side dimensions (L) between 10.7 m and 79.1 m. The
658 separation distance (a) is varied from the center outwards. The solid line is the theoretical error
659 derived for an exponential decay exponent of 0.17 derived from the sampled correlation function
660 of snow depth in FS, while the solid red point markers are the sampled normalized squared error
661 for the snow cover in FS.

662 Figure 16. Theoretical normalized squared error ($\sigma_{\bar{Z}}^2/\sigma_p^2$) for the *N* by *N* point pattern in
663 Figure 12b, and for areas of side dimension (*L*) between 10 and 80. The exponential exponent is
664 varied between 0.1 and 5.

665 Figure 17. Theoretical and sampled normalized squared error ($\sigma_{\bar{Z}}^2/\sigma_p^2$) for the *N* by *N* point
666 pattern in Figure 12b, and over square areas of side dimensions (*L*) between 10.7 m and 79.1 m.
667 The solid black point markers are the theoretical error for an exponential decay exponent of 0.17
668 derived from the sampled correlogram of snow depth in FS. The dotted red lines with circle
669 markers are the sampled normalized squared error for the snow cover in FS.

670

671

672 # References

673 Blöschl, G.: Scaling issues in snow hydrology, *Hydrol. Processes*, *13*(14-15), 2149-2175, 1999.

674 Chang, A. T. C., Kelly, R. E. J., Josberger, E. G., Armstrong, R. L., Foster, J. L., and Mognard,
675 N. M.: Analysis of ground-measured and passive-microwave-derived snow depth variations in
676 midwinter across the northern Great Plains, *J. Hydrometeor., 6*(1), 20-33, doi: 10.1175/Jhm-
677 405.1, 2005.

678 Cline, D., Yueh, S., Chapman, B., Stankov, B., Gasiewski, A., Masters, D., Elder, K., Kelly, R.,
679 Painter, T. H., Miller, S., Katzberg, S., and Mahrt, L.: NASA Cold Land Processes Experiment
680 (CLPX 2002/03): Airborne Remote Sensing, *J. Hydrometeor.*, *10*(1), 338-346, 2009.

681 Cressie, N.: *Statistics for spatial data*, 900 pp., John Wiley & Sons, Inc., USA, 1993.

682 Deems, J. S., Fassnacht, S. R., and Elder, K. J.: Interannual Consistency in Fractal Snow Depth
683 Patterns at Two Colorado Mountain Sites, *J. Hydrometeor., 9*(5), 977-988, doi:
684 10.1175/2008jhm901.1, 2008.

685 Grünewald, T., and Lehning, M.: Are flat-field snow depth measurements representative? A
686 comparison of selected index sites with areal snow depth measurements at the small catchment
687 scale, *Hydrol. Processes*, doi: 10.1002/hyp.10295, 2014.

688 Helfrich, K., Schöber, J., Schneider, K., Sailer, R., and Kuhn, M.: Interannual persistence of the
689 seasonal snow cover in a glacierized catchment, *J. Glaciol., 60*(223), 889-904, doi:
690 10.3189/2014JoG13J197, 2014.

691 Journel, A. G., and Huijbregts, C. J.: *Mining Geostatistics*, Academic Press, London, 1978.

692 Kronholm, K., and Birkeland, K. W.: Reliability of sampling designs for spatial snow surveys,
693 *Comput. Geosci.*, *33*(9), 1097-1110, 2007.

694 Lopez-Moreno, J. I., Fassnacht, S. R., Begueria, S., and Latron, J. B. P.: Variability of snow
695 depth at the plot scale: implications for mean depth estimation and sampling strategies,
696 *Cryosphere*, *5*(3), 617-629, 2011.

697 Matheron, G.: Application des méthodes statistiques à l'estimation des gisements, *Annales de*
698 *Mines*, *Dec*, 50-75, 1955.

699 Matheron, G.: Random functions, and their applications in geology, in *Geostatistics - A*
700 *colloquium*, edited by D. Merriam, pp. 79-87, Plenum Press, New York, 1970.

701 McCreight, J. L., Slater, A. G., Marshall, H. P., and Rajagopalan, B.: Inference and uncertainty
702 of snow depth spatial distribution at the kilometre scale in the Colorado Rocky Mountains: the
703 effects of sample size, random sampling, predictor quality, and validation procedures, *Hydrol.*
704 *Processes*, *28*(3), 933-957, 2014.

705 Melvold, K., and Skaugen, T.: Multiscale spatial variability of lidar-derived and modeled snow
706 depth on Hardangervidda, Norway, *Ann. Glaciol.*, *54*(62), 273-281, 2013.

707 Meromy, L., Molotch, N. P., Link, T. E., Fassnacht, S. R., and Rice, R.: Subgrid variability of
708 snow water equivalent at operational snow stations in the western USA, *Hydrol. Processes,*
709 *27*(17), 2383-2400, doi: 10.1002/Hyp.9355, 2013.

710 Mott, R., Schirmer, M., and Lehning, M.: Scaling properties of wind and snow depth distribution
711 in an Alpine catchment, *Journal of Geophysical Research: Atmospheres, 116*(D6), D06106, doi:
712 10.1029/2010jd014886, 2011.

713 Pomeroy, J. W., and Gray, D. M.: *Snow Accumulation, Relocation and Management (NHRI*
714 *Science Report No. 7)*, Environment Canada, Saskatoon, 1995.

715 Rice, R., and Bales, R. C.: Embedded-sensor network design for snow cover measurements
716 around snow pillow and snow course sites in the Sierra Nevada of California, *Water Resour.*
717 *Res., 46*, W03537, doi: 10.1029/2008wr007318, 2010.

718 Rodríguez-Iturbe, I., and Mejía, J. M.: Design of Rainfall Networks in Time and Space, *Water*
719 *Resour. Res.*, *10*(4), 713-728, 1974.

720 Schirmer, M., Wirz, V., Clifton, A., and Lehning, M.: Persistence in intra-annual snow depth
721 distribution: 1. Measurements and topographic control, *Water Resour. Res., 47*(9), W09516, doi:
722 10.1029/2010wr009426, 2011.

723 Shea, C., and Jamieson, B.: Star: an efficient snow point-sampling method, *Ann. Glaciol.*,
724 *51*(54), 64-72, 2010.

725 Skøien, J. O., and Blöschl, G.: Sampling scale effects in random fields and implications for
726 environmental monitoring, *Environ. Monit. Assess., 114*(1-3), 521-552, doi: Doi
727 10.1007/S10661-006-4939-Z, 2006.

728 Sturm, M., and Wagner, A. M.: Using repeated patterns in snow distribution modeling: An
729 Arctic example, *Water Resour. Res.*, *46*, 2010.

730 Trujillo, E., Ramirez, J. A., and Elder, K. J.: Topographic, meteorologic, and canopy controls on
731 the scaling characteristics of the spatial distribution of snow depth fields, *Water Resour. Res., 43*,
732 W07409, doi: 10.1029/2006WR005317, 2007.

733 Trujillo, E., Ramírez, J. A., and Elder, K. J.: Scaling properties and spatial organization of snow
734 depth fields in sub-alpine forest and alpine tundra, *Hydrol. Processes, 23*, 1575–1590, doi:
735 10.1002/hyp.7270, 2009.

736 Watson, F. G. R., Anderson, T. N., Newman, W. B., Alexander, S. E., and Garrott, R. A.:
737 Optimal sampling schemes for estimating mean snow water equivalents in stratified
738 heterogeneous landscapes, *J. Hydrol., 328*(3-4), 432-452, doi: 10.1016/J.Jhydrol.2005.12.032,
739 2006.

740 Yang, D. Q., and Woo, M. K.: Representativeness of local snow data for large scale hydrologic
741 investigations, *Hydrol. Processes, 13*(12-13), 1977-1988, doi: 10.1002/(Sici)1099-
742 1085(199909)13:12/13<1977::Aid-Hyp894>3.0.Co;2-B, 1999.

743

744

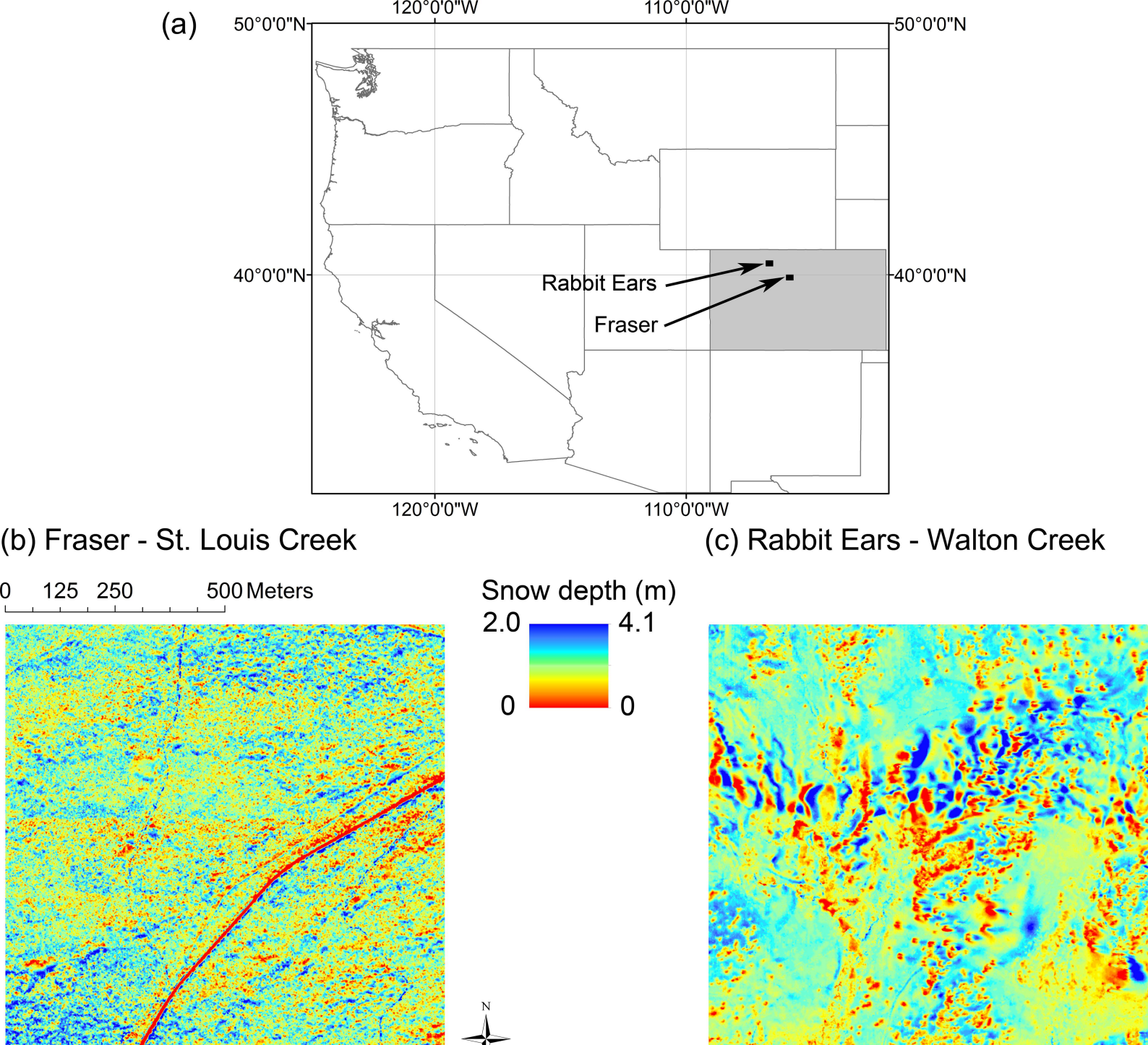
(a)
120°0'0"W
110°0'0"W
50°0'0"N
40°0'0"N
Rabbit Ears
Fraser
(b) Fraser - St. Louis Creek
(c) Rabbit Ears - Walton Creek
0 125 250 500 Meters
Snow depth (m)
2.0
4.1
0
0
N

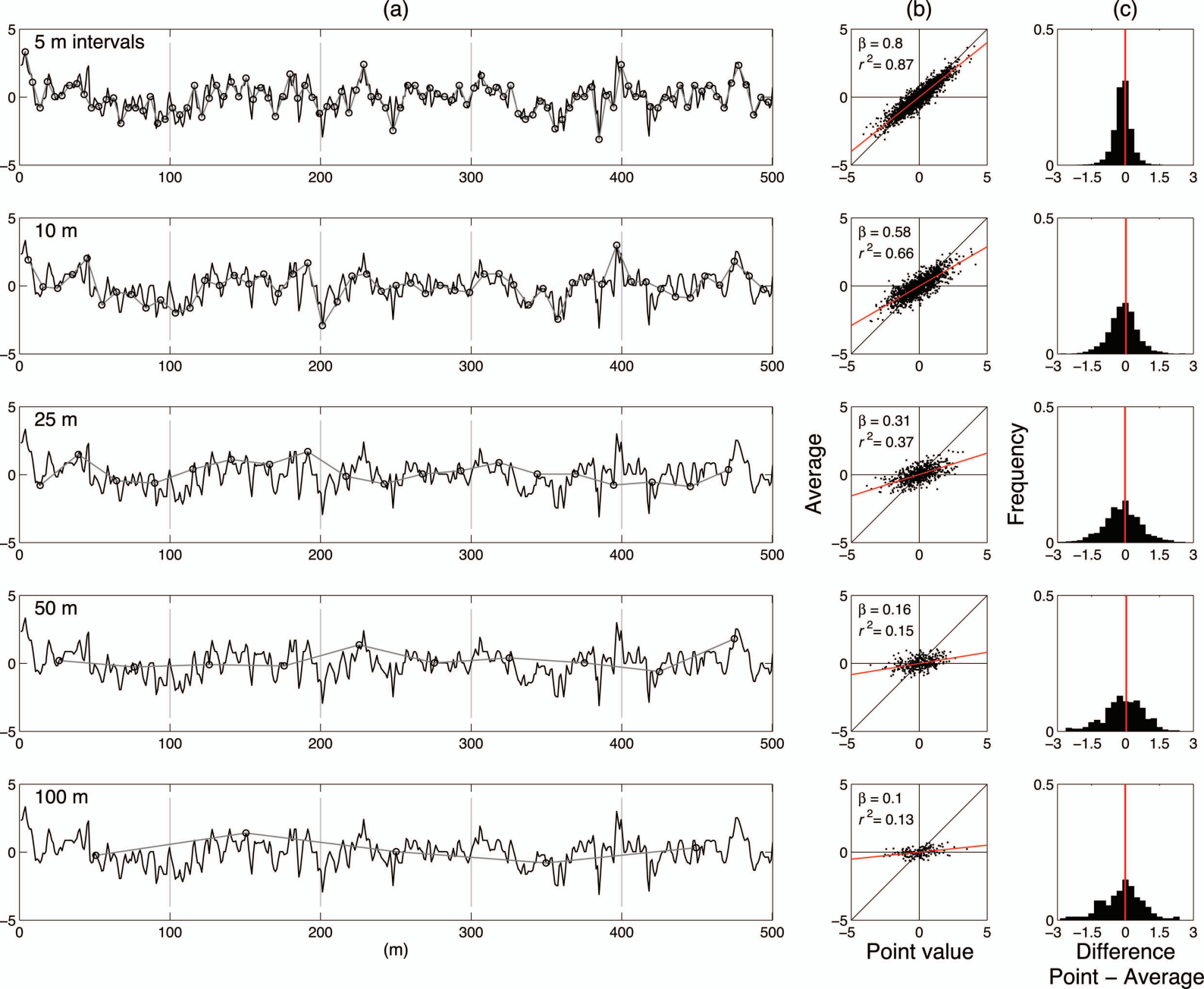
(a)
(b)
(c)
5 m intervals
10 m
25 m
50 m
100 m
β = 0.8
r 2 = 0.87
β = 0.58
r 2 = 0.66
β = 0.31
r 2 = 0.37
β = 0.16
r 2 = 0.15
β = 0.1
r 2 = 0.13
Average
Frequency
(m)
Point value
Difference
Point – Average

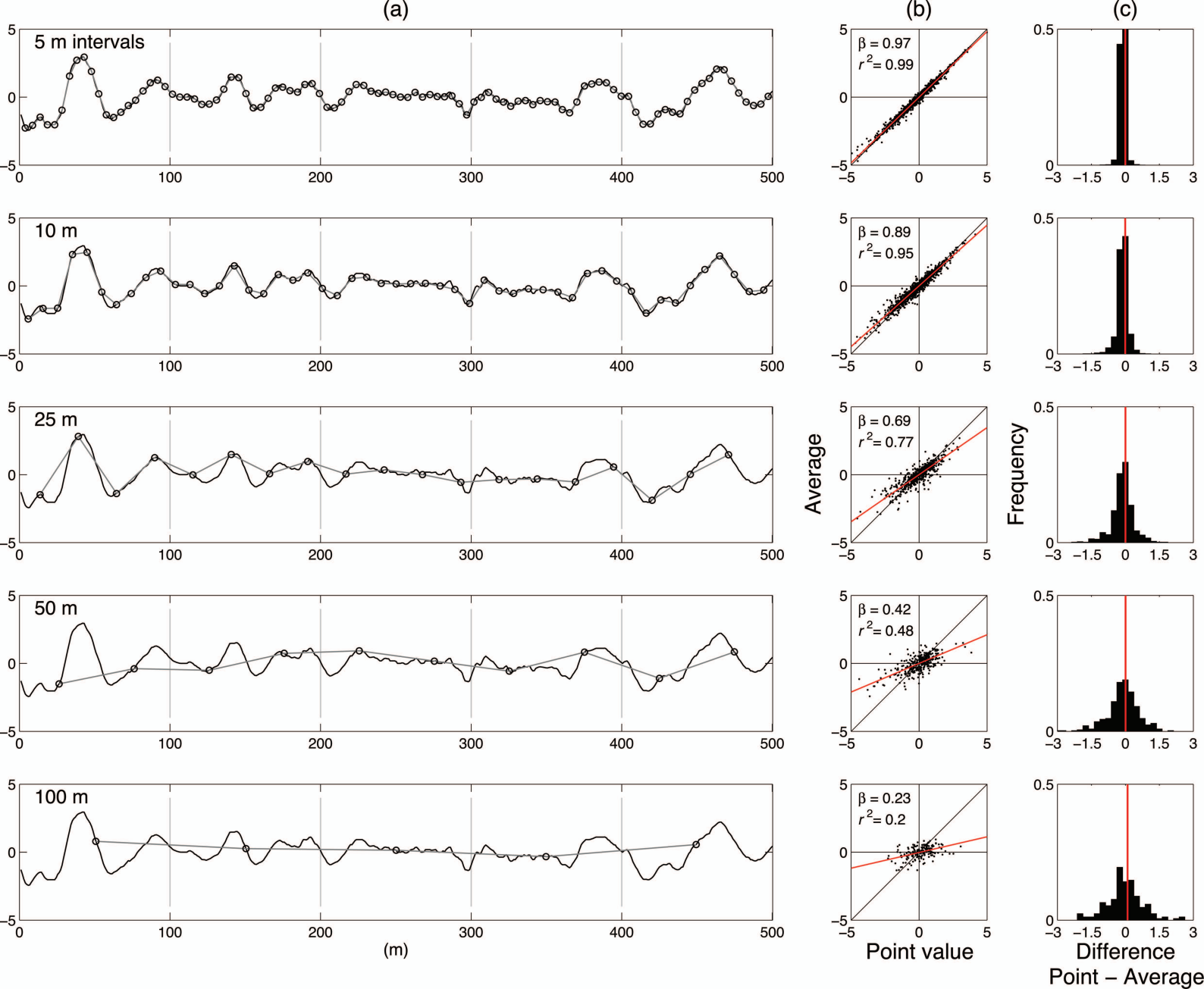
(a)
(b)
(c)
5 m intervals
10 m
25 m
50 m
100 m
β = 0.97
r 2 = 0.99
β = 0.89
r 2 = 0.95
β = 0.69
r 2 = 0.77
β = 0.42
r 2 = 0.48
β = 0.23
r 2 = 0.2
Average
Frequency
(m)
Point value
Difference
Point – Average

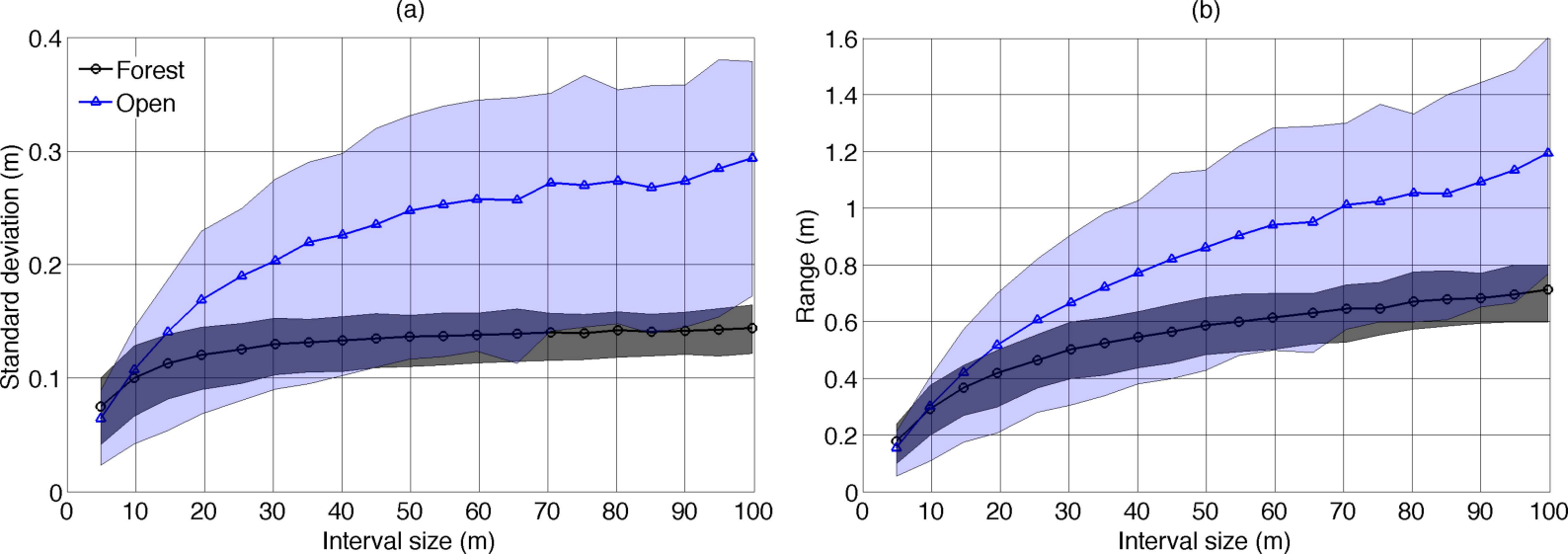
(a)
(b)
Forest
Open
Standard deviation (m)
Range (m)
Interval size (m)
Interval size (m)
0
0.1
0.2
0.3
0.4
0.6
0.8
1
1.2
1.4
1.6
10
20
30
40
50
60
70
80
90
100

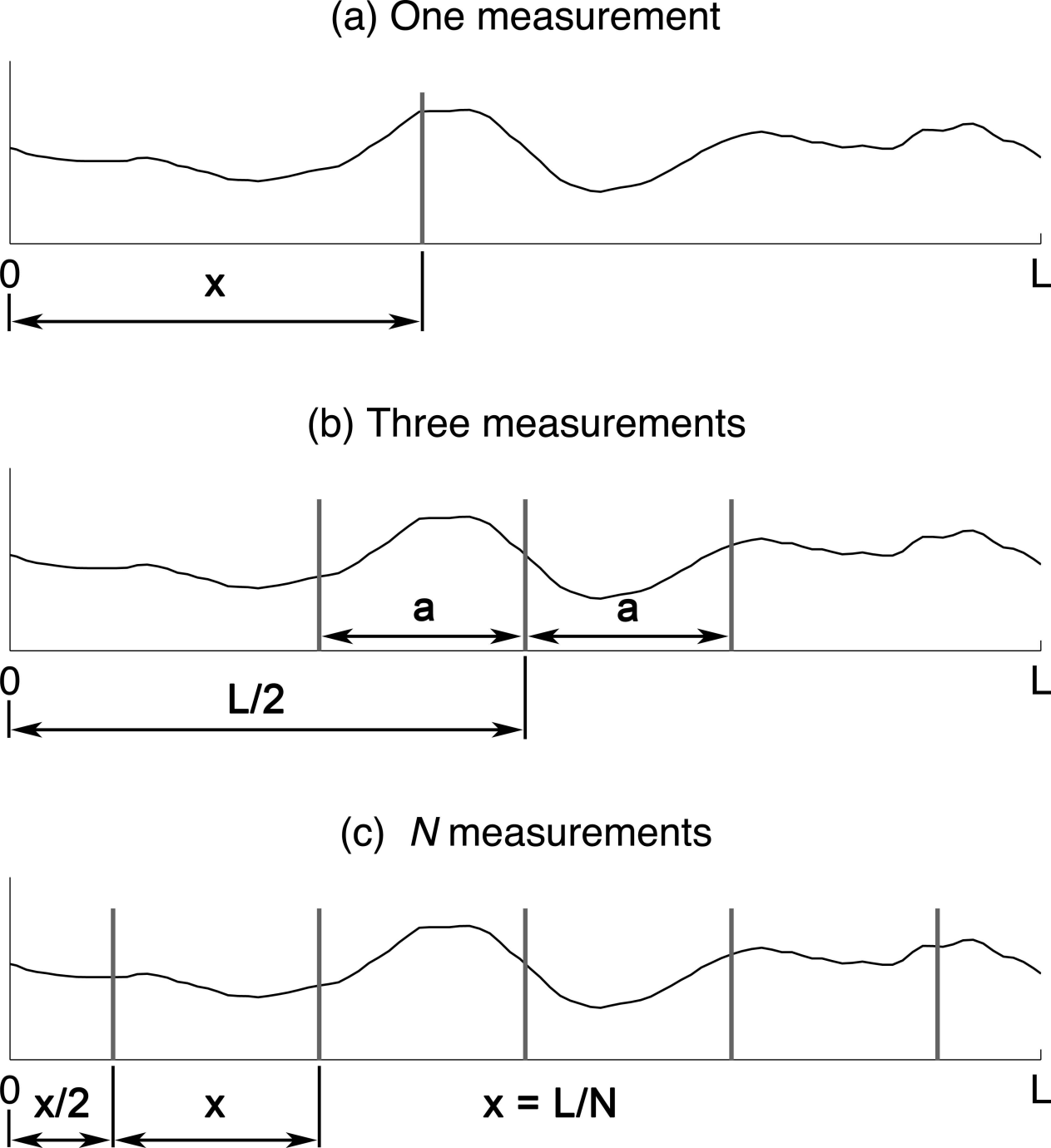
(a) One measurement
0
x
L
(b) Three measurements
a
a
0
L/2
L
(c) N measurements
0
x/2
x
x = L/N
L

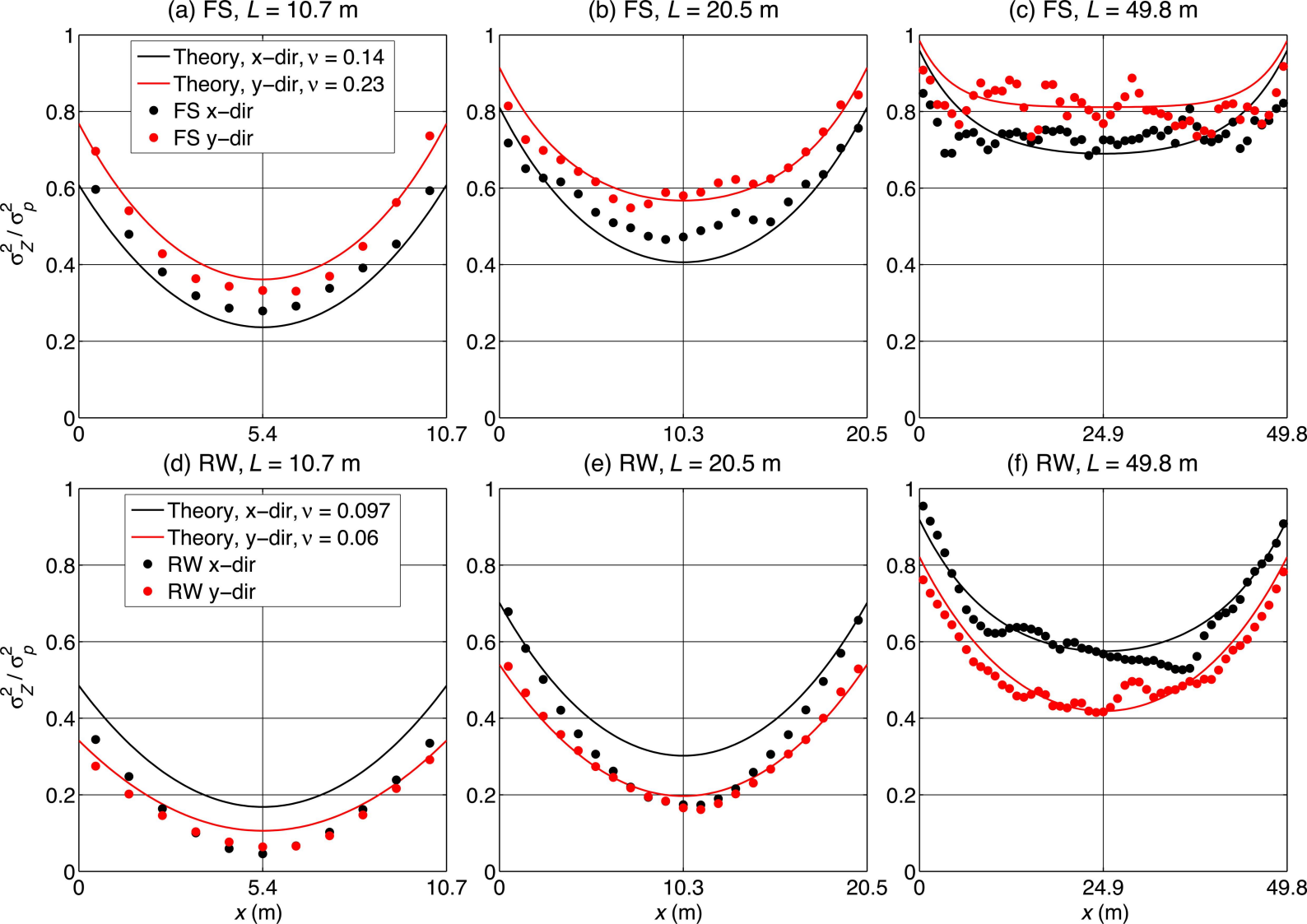
(a) FS, L = 10.7 m
(b) FS, L = 20.5 m
(c) FS, L = 49.8 m
(d) RW, L = 10.7 m
(e) RW, L = 20.5 m
(f) RW, L = 49.8 m
Theory, x–dir, ν = 0.14
Theory, y–dir, ν = 0.23
FS x–dir
FS y–dir
Theory, x–dir, ν = 0.097
Theory, y–dir, ν = 0.06
RW x–dir
RW y–dir
σ²Z / σ²p
x (m)
0
5.4
10.7
10.3
20.5
24.9
49.8
0.2
0.4
0.6
0.8
1

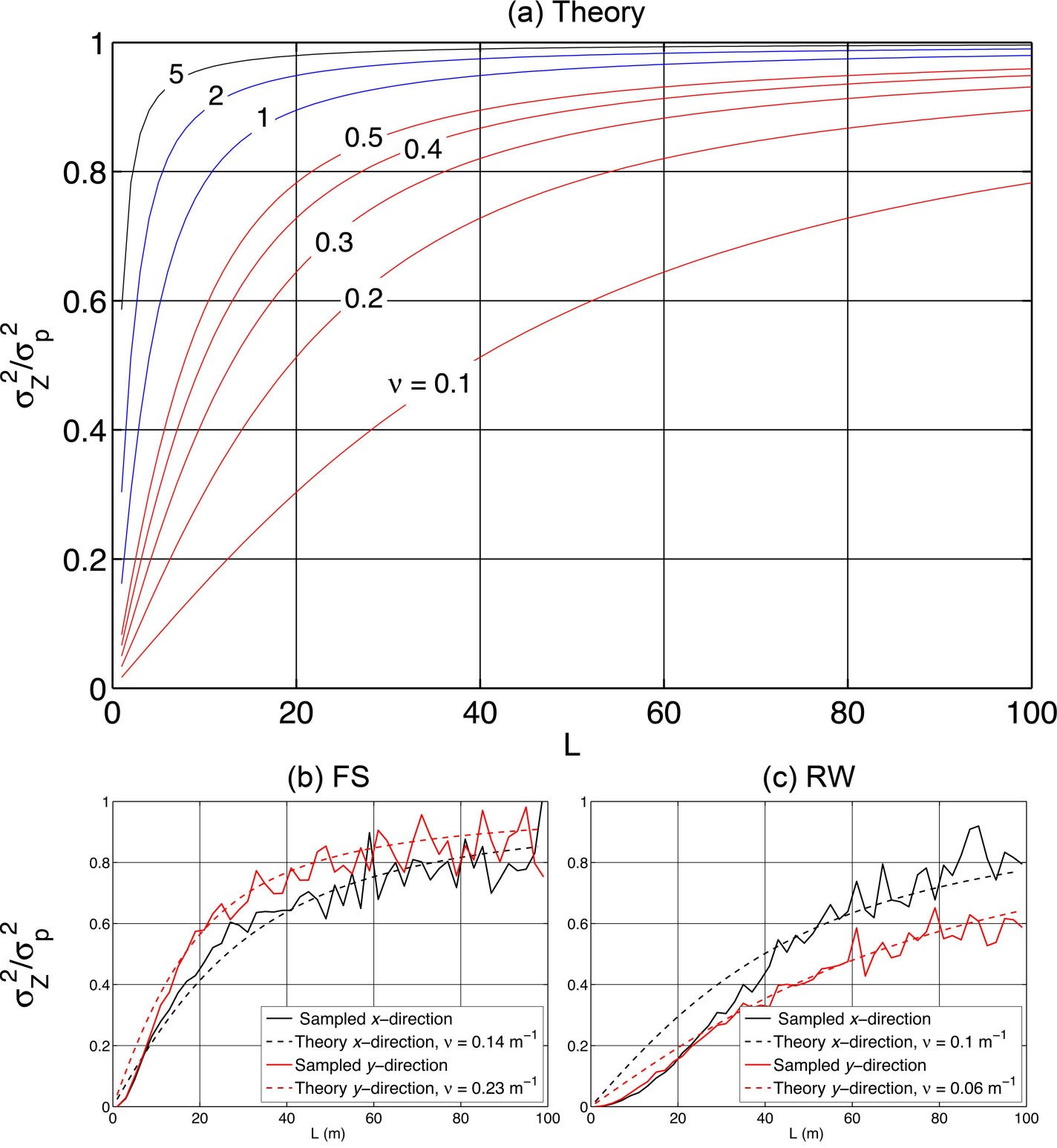
(a) Theory
σ_Z^2/σ_p^2
L
5
2
1
0.5
0.4
0.3
0.2
ν = 0.1
(b) FS
Sampled x–direction
Theory x–direction, ν = 0.14 m^{-1}
Sampled y–direction
Theory y–direction, ν = 0.23 m^{-1}
L (m)
(c) RW
Sampled x–direction
Theory x–direction, ν = 0.1 m^{-1}
Sampled y–direction
Theory y–direction, ν = 0.06 m^{-1}
L (m)

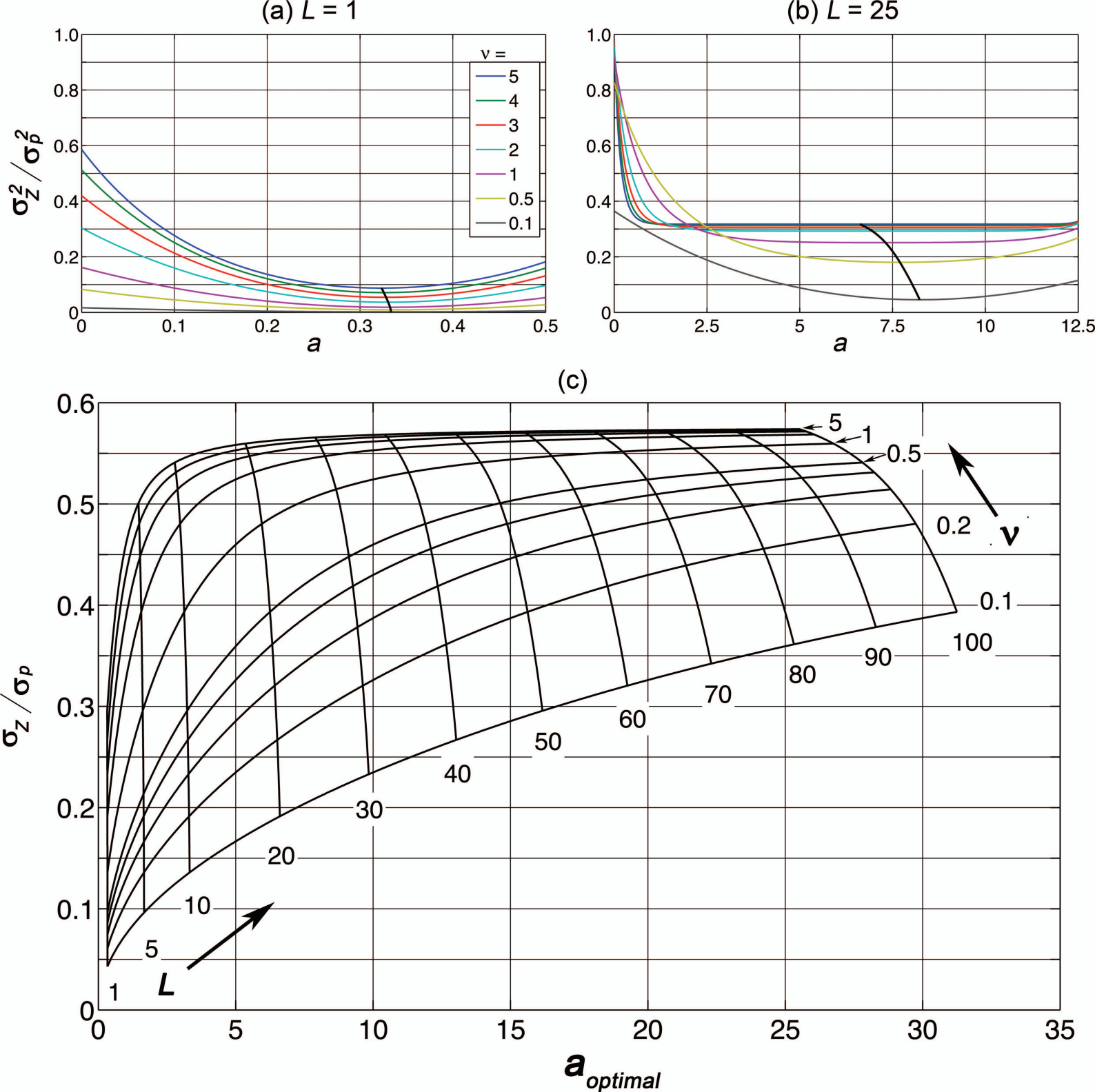
(a) L = 1
(b) L = 25
(c)
ν =
5
4
3
2
1
0.5
0.1
σ_Z^2 / σ_p^2
a
σ_Z / σ_p
a_optimal
L
ν
1
5
10
20
30
40
50
60
70
80
90
100
0.2
0.1
0.5

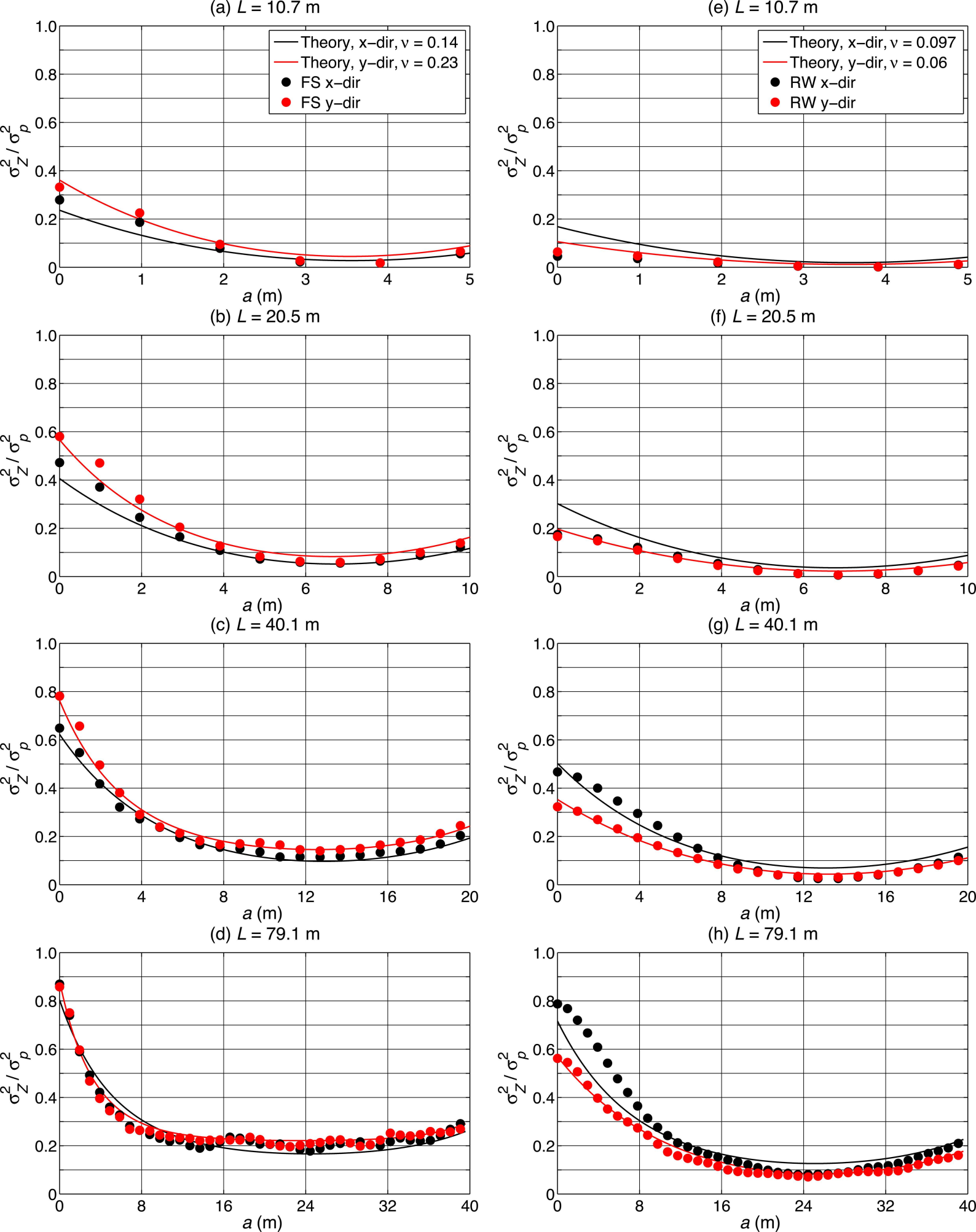
(a) L = 10.7 m
Theory, x–dir, ν = 0.14
Theory, y–dir, ν = 0.23
FS x–dir
FS y–dir
(e) L = 10.7 m
Theory, x–dir, ν = 0.097
Theory, y–dir, ν = 0.06
RW x–dir
RW y–dir
(b) L = 20.5 m
(f) L = 20.5 m
(c) L = 40.1 m
(g) L = 40.1 m
(d) L = 79.1 m
(h) L = 79.1 m
σ²Z / σ²p
a (m)

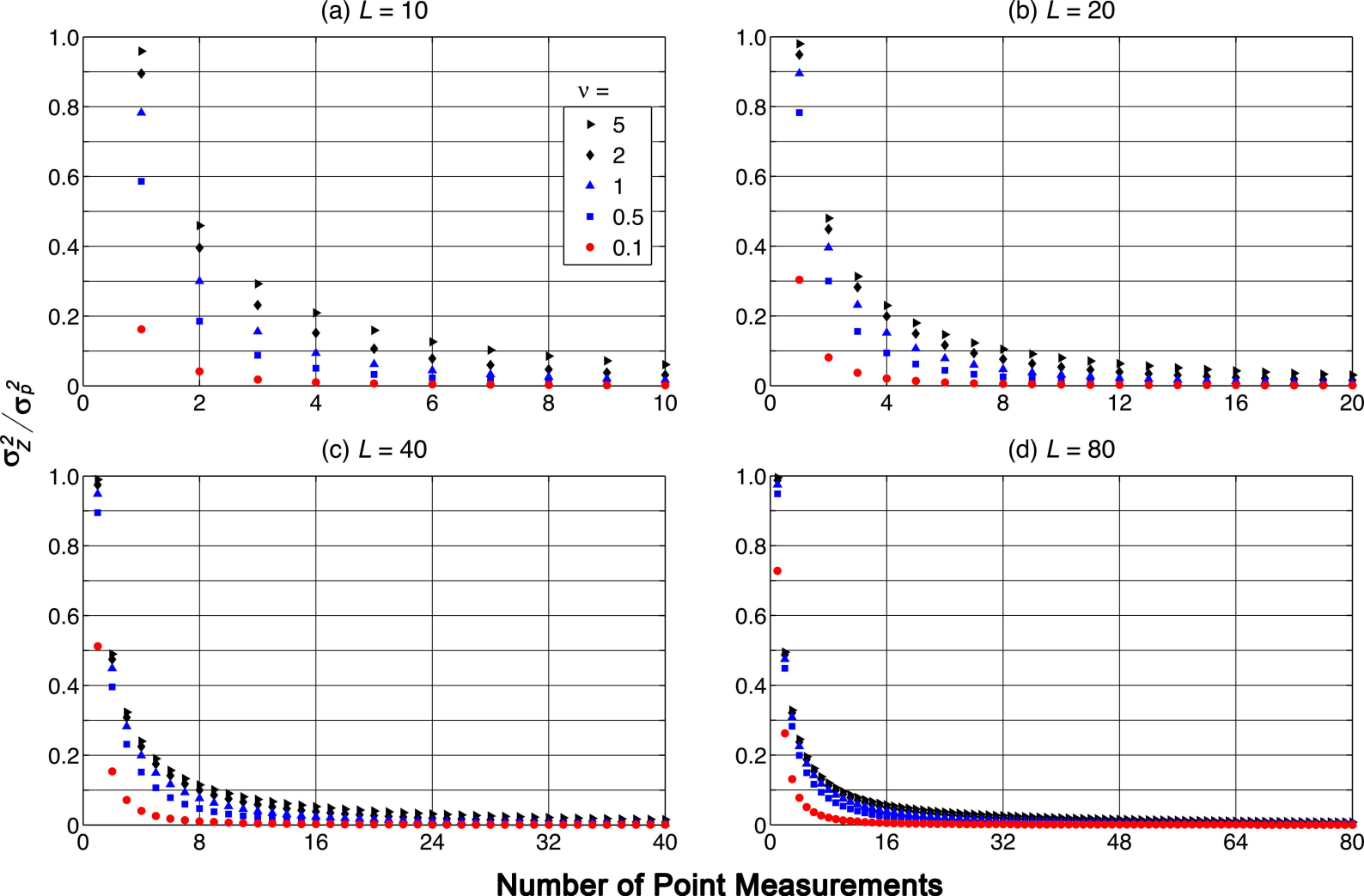
(a) L = 10
(b) L = 20
(c) L = 40
(d) L = 80
ν =
5
2
1
0.5
0.1
σ²Z / σ²p
Number of Point Measurements

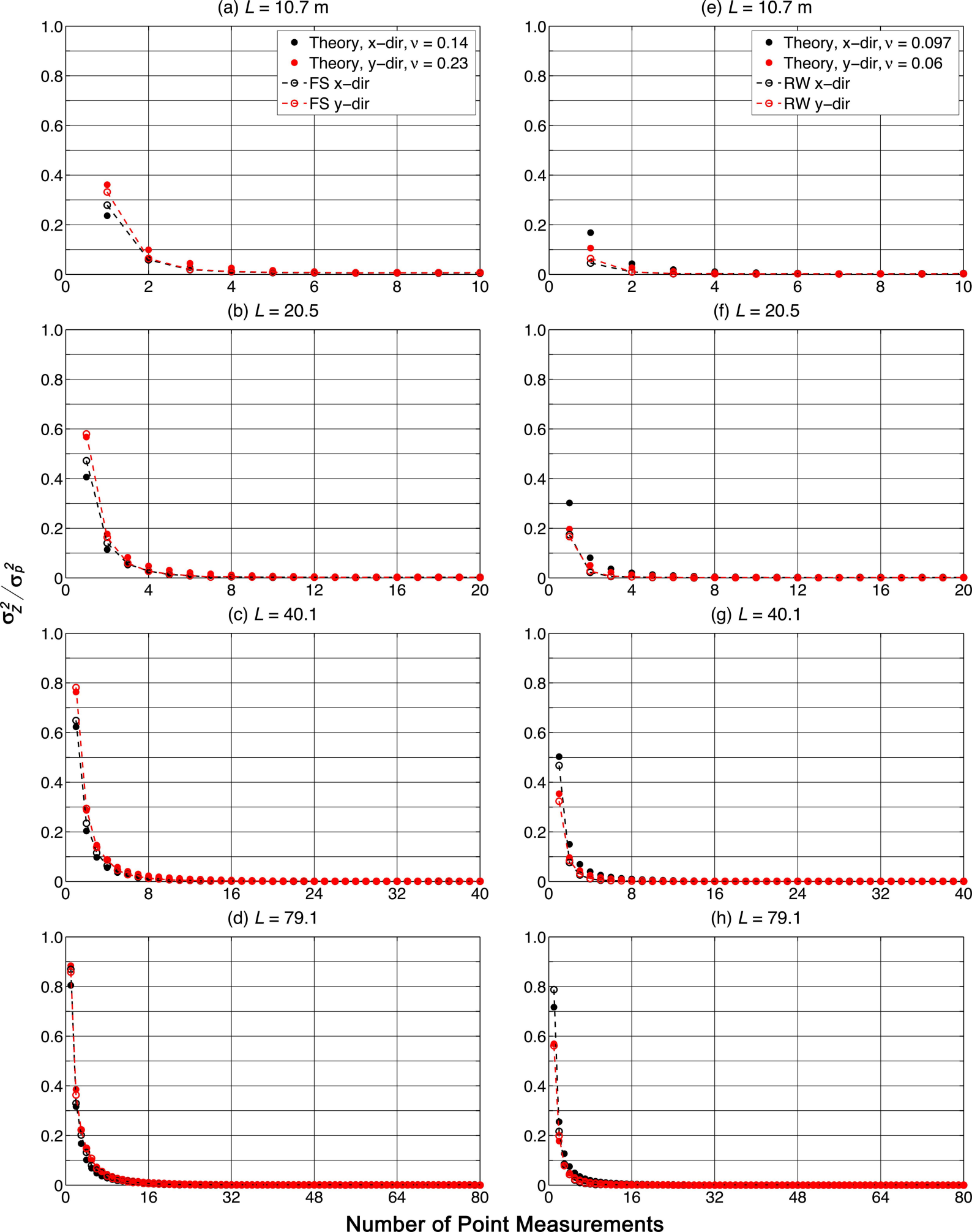
(a) L = 10.7 m
(e) L = 10.7 m
Theory, x–dir, ν = 0.14
Theory, y–dir, ν = 0.23
FS x–dir
FS y–dir
Theory, x–dir, ν = 0.097
Theory, y–dir, ν = 0.06
RW x–dir
RW y–dir
(b) L = 20.5
(f) L = 20.5
(c) L = 40.1
(g) L = 40.1
(d) L = 79.1
(h) L = 79.1
σ²Z / σ²p
Number of Point Measurements

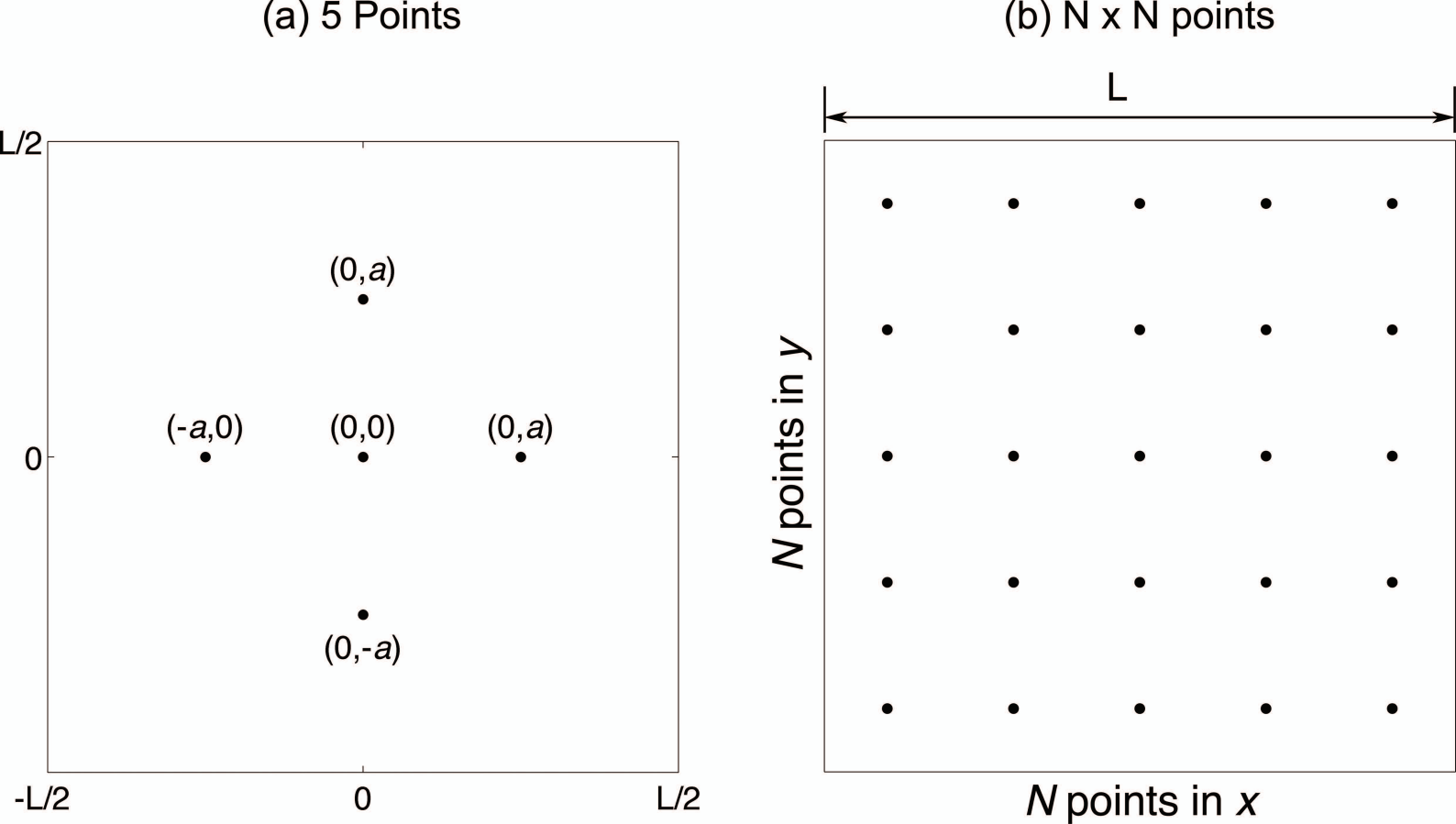
(a) 5 Points
L/2
0
-L/2
0
L/2
(0,a)
(-a,0)
(0,0)
(0,a)
(0,-a)
(b) N x N points
L
N points in y
N points in x

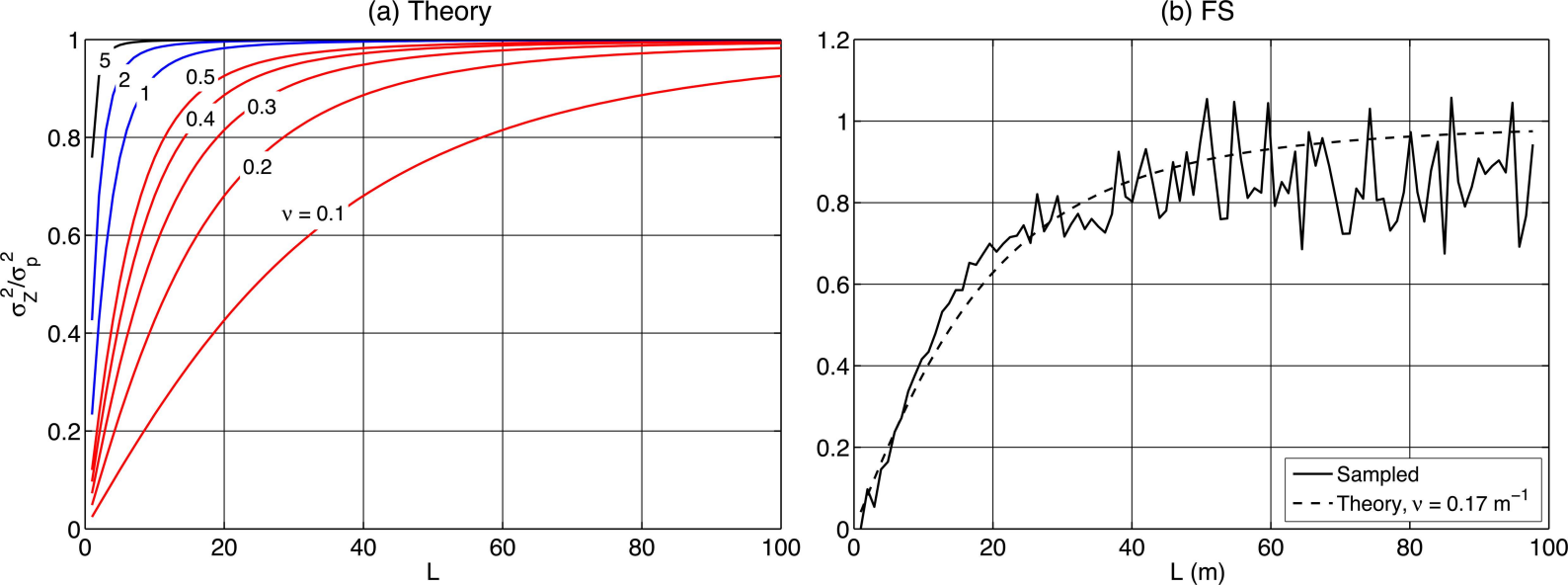
(a) Theory
(b) FS
σ_Z^2/σ_p^2
L
L (m)
5
2
1
0.5
0.4
0.3
0.2
ν = 0.1
Sampled
Theory, ν = 0.17 m^{-1}

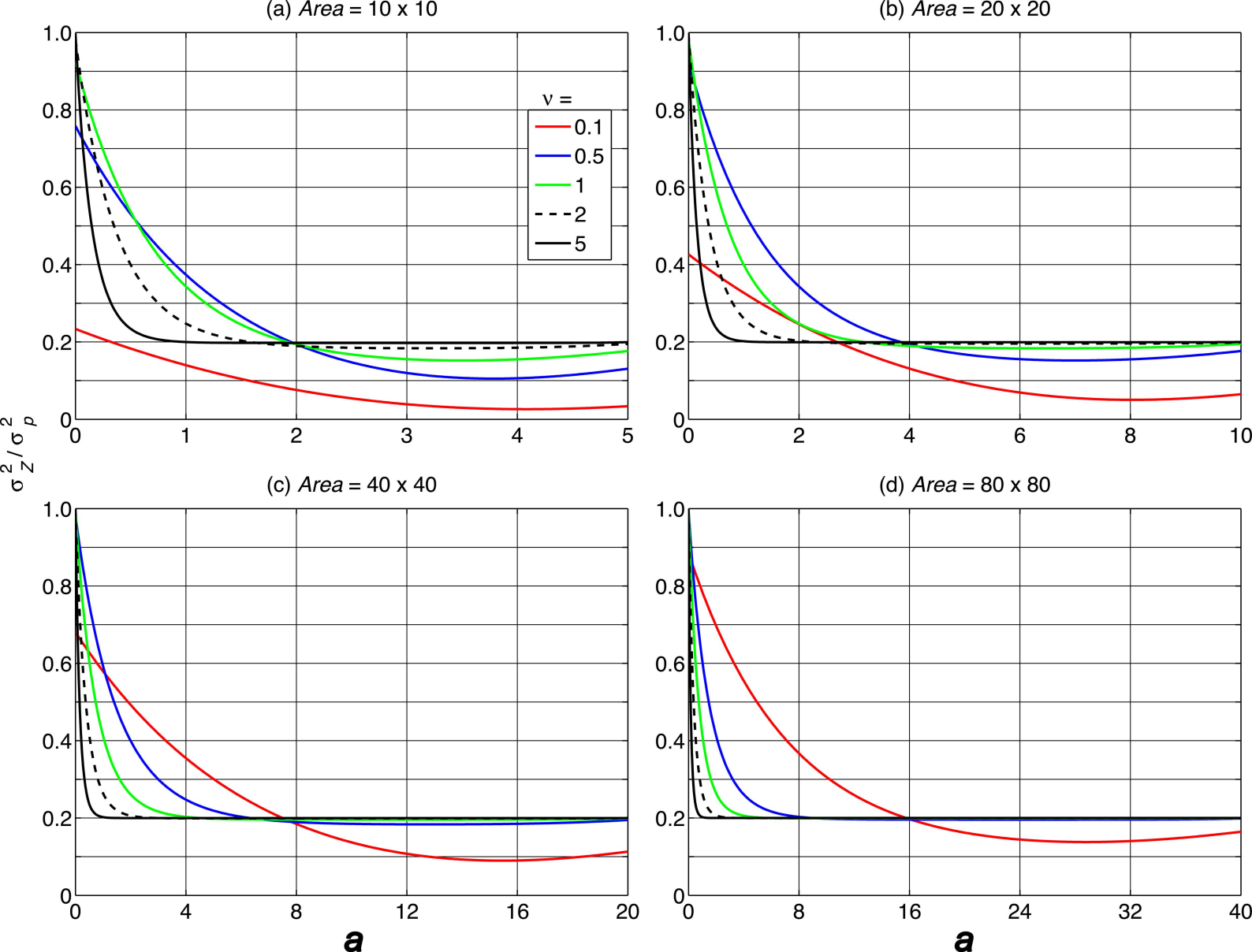
(a) Area = 10 x 10
(b) Area = 20 x 20
(c) Area = 40 x 40
(d) Area = 80 x 80
ν =
0.1
0.5
1
2
5
σ²Z / σ²p
a
a

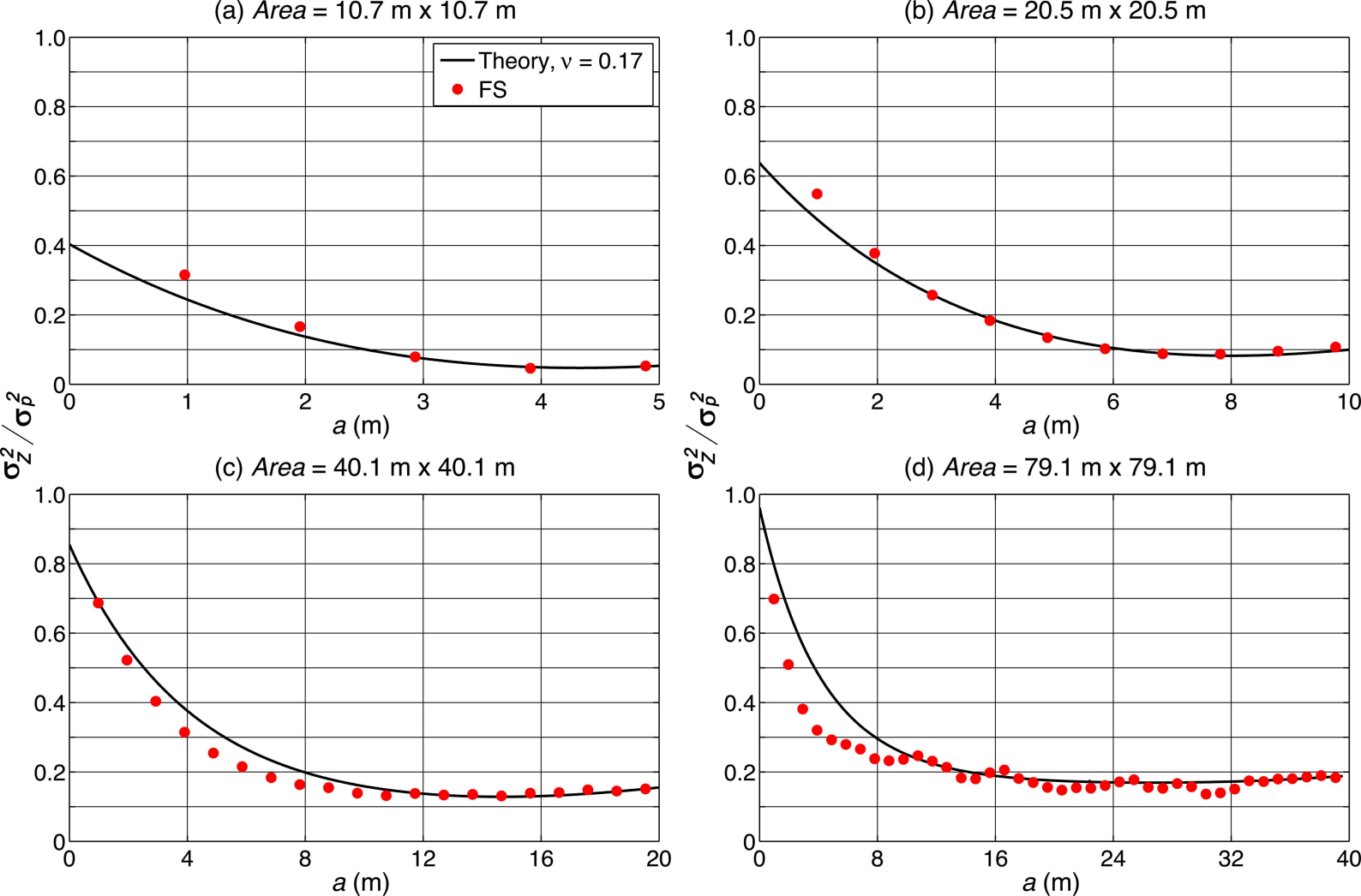
(a) Area = 10.7 m x 10.7 m
(b) Area = 20.5 m x 20.5 m
(c) Area = 40.1 m x 40.1 m
(d) Area = 79.1 m x 79.1 m
Theory, ν = 0.17
FS
σ²Z / σ²p
a (m)
0
0.2
0.4
0.6
0.8
1.0
1
2
3
4
5
6
8
10
12
16
20
24
32
40

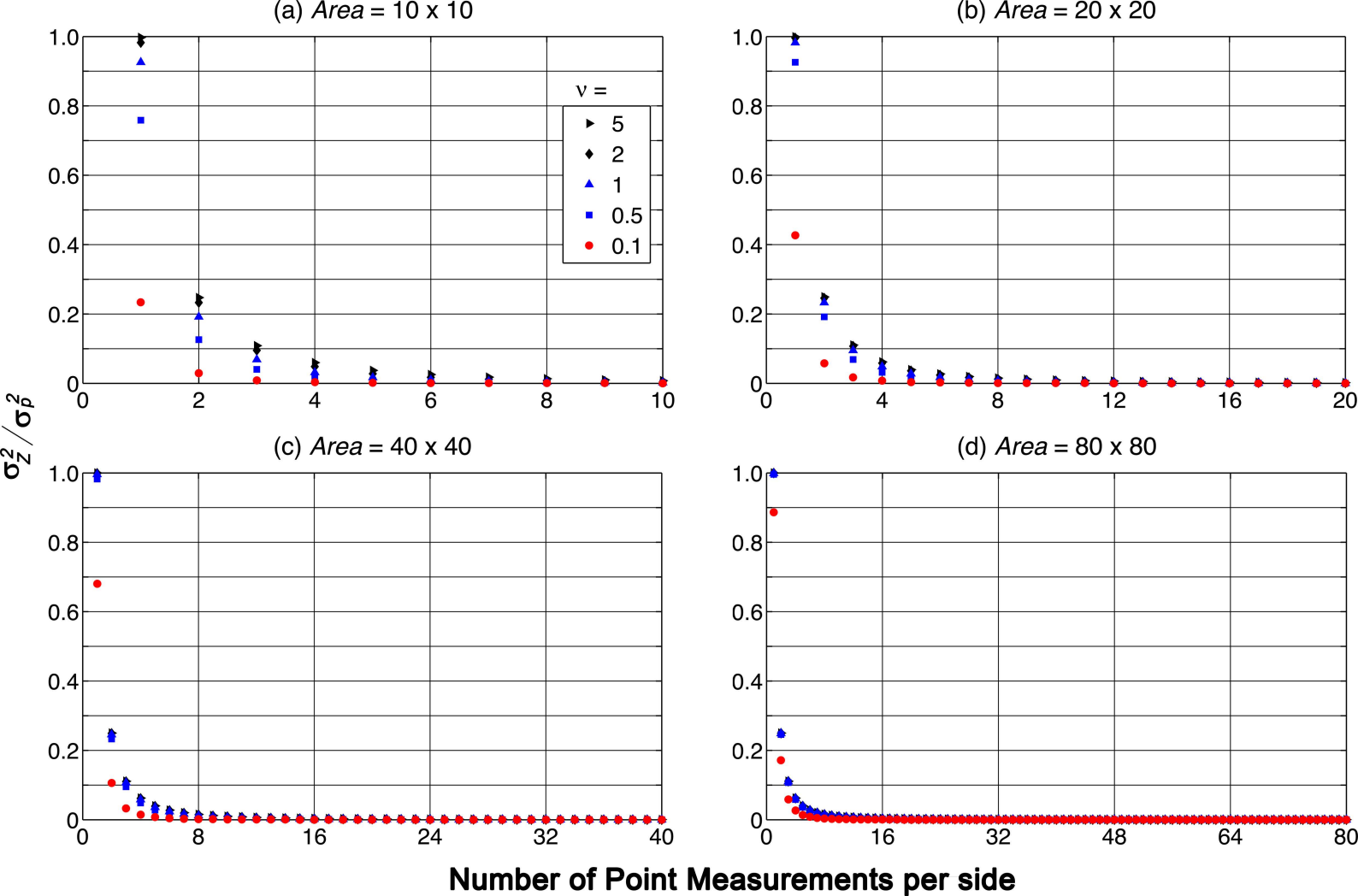
(a) Area = 10 x 10
(b) Area = 20 x 20
(c) Area = 40 x 40
(d) Area = 80 x 80
ν =
5
2
1
0.5
0.1
σ_Z^2/σ_p^2
Number of Point Measurements per side

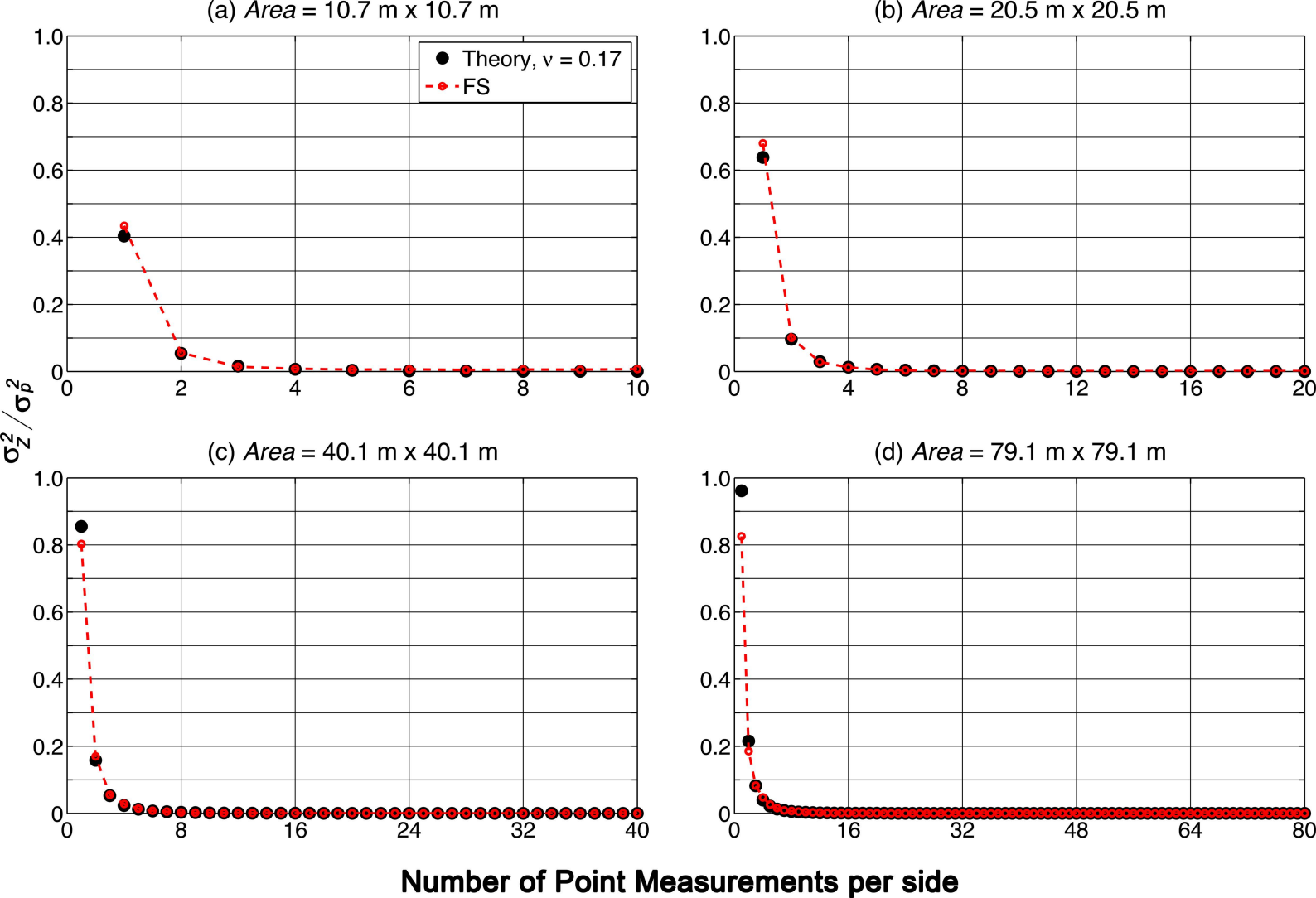
(a) Area = 10.7 m x 10.7 m
(b) Area = 20.5 m x 20.5 m
(c) Area = 40.1 m x 40.1 m
(d) Area = 79.1 m x 79.1 m
Theory, ν = 0.17
FS
σ²Z / σ²p
Number of Point Measurements per side